

**DETECTION OF DNA HYBRIDIZATION AND
DEHYBRIDIZATION WITH SURFACE ENHANCED RAMAN
SPECTROSCOPY (SERS) BY USING GOLD NANOVoids
ELECTRODES**

**DNA HİBRİDİZASYONU VE DEHİBRİDİZASYONUNUN
ALTIN NANOBOŞLUKLU ELEKTROTLAR KULLANARAK
YÜZEYDE ZENGİNLEŞTİRİLMİŞ RAMAN (SERS)
SPEKTROSKOPİSİ İLE TAYİNİ**

NERGİS ÇINAR

Prof. Dr. HANDAN YAVUZ ALAGÖZ
Supervisor

Submitted to Graduate School of Science and Engineering of Hacettepe University
as a Partial Fulfillment to the Requirements
for the Award of the Degree of Master of Science
in Chemistry

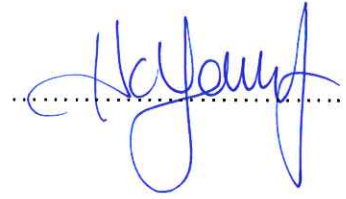
2017

This work named “**Detection of DNA Hybridization and Dehybridization With Surface Enhanced Raman Spectroscopy (SERS) By Using Gold Nanovoids Electrodes**“ by **Nergis ÇINAR** has been approved as a thesis for the Degree of **MASTER OF SCIENCE IN CHEMISTRY** by the below mentioned Examining Committee Members.

Prof. Dr. Adil DENİZLİ
Head



Prof. Dr. Handan YAVUZ ALAGÖZ
Supervisor



Assoc. Prof. Dr. Nilay BERELİ
Member



Assist. Prof. Dr. Ceren HAKTANIR
Member



Assist. Prof. Dr. Fatma Yılmaz
Member



This thesis has been approved as a thesis for the Degree of **MASTER OF SCIENCE IN CHEMISTRY** by Board of the Institute for Graduate School of Science and Engineering.

Prof. Dr. Menemşe GÜMÜŞDERELİOĞLU
Director of the Institute of
Graduate School of Science and Engineering

To my family

ETHICS

In this thesis study, prepared in accordance with the spelling rules of Institute of Graduate Studies in Science of Hacettepe University,

I declare that

- all the information and documents have been obtained in the base of academic rules
- all audio-visual and written information and results have been presented according to the rules of scientific ethics
- in case of using others Works, related studies have been cited in accordance with the scientific standards
- all cited studies have been fully referenced
- I did not do any distortion in the data set
- And any part of this thesis has not been presented as another thesis study at this or any other university.

20/01/2017



Nergis ÇINAR

ÖZET

DNA HİBRİDİZASYONU VE DEHİBRİDİZASYONUNUN ALTIN NANOBOŞLUKLU ELEKTROTLAR KULLANARAK YÜZEYDE ZENGİNLEŞTİRİLMİŞ RAMAN (SERS) SPEKTROSKOPİSİ İLE TAYİNİ

NERGİS ÇINAR

Yüksek Lisans, Kimya Bölümü

Tez Danışmanı: Prof. Dr. Handan YAVUZ ALAGÖZ

Ocak 2017, 55 sayfa

Yaklaşık olarak her 30 baz çiftinde tek nokta polimorfizmi (SNP) bulunabilir. Dolayısıyla SNP'lerin hızlı ve hassas şekilde tespit edilmesi önemlidir. Bu nedenle, tezde tek nokta polimorfizmi (SNP) tayini için yüzeyde zenginleştirilmiş Raman spektroskopisine dayalı DNA sensörü geliştirilmesine odaklanılmıştır. Çalışma üç aşamada gerçekleştirilmiştir. İlk adım, SERS substratlarının hazırlanması ve yüksek hassasiyet elde etmek üzere bu substratların optimizasyonudur. Pürüzsüz Au plakakar Langmuir-Blodgett yöntemi kullanılarak polistiren küreler ile kaplanmıştır. Ardından nanoyapıları oluşturmak için elektrokimyasal Au kaplanması gerçekleştirilmiştir. Optimal Au kalınlığını belirlemek üzere Au kalınlık gradyanı oluşturmak için bipolar elektrokimya kullanılmıştır. Bipolar elektrotlar 4-nitrothiofenol (4-NTP) ile modifiye edilmiş ve elektrotlar boyunca sinyal yoğunlukları SERS kullanılarak tespit edilmiştir. 200 nm çaplı polistiren küreler 177.8 nm Au kalınlığı ile en yüksek sinyal sağlamıştır.

İkinci adımda, optimize edilmiş SERS substratları üzerinde potansiyel destekli immobilizasyon yöntemi ile bir algılama platformu oluşturulmuştur. Hazırlanan sensörler tamamen eşleşen hedef DNA ile hibridize edilmiş ve elektrokimyasal DNA erime kinetiği, in-situ Raman ölçümleri ile izlenmiştir. Daha sonra, ssDNA desorpsiyon kinetikleri de in-situ Raman ölçümleri ile analiz edilmiştir.

Elektrokimyasal erime potansiyeli başlangıcı Ag/AgCl (3 M KCl) için -1100 mV, ve ssDNA desorpsiyon başlangıcı Ag/AgCl (3 M KCl) için -1300 mV'de olduğu için dsDNA dehidridizasyonu için Ag/AgCl (3 M KCl) için -1250 mV seçilmiştir. Son adımda, SNP tespiti, uygulanan potansiyel nedeniyle zamanla sinyal azalması izlenerek gerçekleştirilmiştir. Modifiye edilmiş SERS substratlar, tek eşleşmeyen hedef DNA ve tamamen eşleşen hedef DNA ile ayrı ayrı hibridize edilmiştir. Potansiyel yardımcı DNA erimesi in-situ Raman ölçümleri ile izlenmiştir. Sonuçlar SNP içeren hedef DNA'dan gelen sinyalin % 60'ının 60 saniye erime sonrasında kaybolduğunu ortaya koyarken, tam olarak eşleşen hedef DNA'nın sadece %10'u aynı zaman süresinde dehidridize edilmiştir. Tasarlanan sensörün tekrarlanabilirliği de tatmin edicidir.

Anahtar kelimeler: DNA biyosensörü, YGRS, Langmuir-Blodgett, bipolar elektrokimya, potansiyel destekli, erime noktası.

ABSTRACT

DETECTION OF DNA HYBRIDIZATION AND DEHYBRIDIZATION WITH SURFACE ENHANCED RAMAN SPECTROSCOPY (SERS) BY USING GOLD NANOVoids ELECTRODES

NERGİS ÇINAR

Master of Science; Department of Chemistry

Supervisor: Prof. Dr. HANDAN YAVUZ ALAGÖZ

January 2017, 55 pages

Approximately every 30 base pairs may contain an SNP. Thus rapid and sensitive detection of SNPs is essential. Therefore, this thesis was focused on the development of a DNA sensor with the surface enhanced Raman spectroscopy based detection of single nucleotide polymorphism (SNP). The study was accomplished in three steps. The first step was the preparation of the SERS substrates and their optimization in order to obtain high sensitivity. Smooth Au wafers were covered with polystyrene beads using the Langmuir-Blodgett method. Subsequently, electrochemical Au deposition was performed to form the nanostructures. In order to determine the optimal Au thickness the bipolar electrochemistry was employed to form an Au thickness gradient. The bipolar electrodes were modified with 4-nitrothiophenol (4-NTP), and the signal intensities along the bipolar electrodes were detected using SERS. The polystyrene spheres with 200 nm diameter provided the highest signal enhancement with 177.8 nm Au thickness.

The second step was the formation of a sensing platform by means of the potential-assisted immobilization method on optimized SERS substrates. The

prepared sensors were then hybridized with fully-matched target DNA and the electrochemical DNA melting kinetics was monitored via in-situ Raman measurements. Furthermore, the ssDNA desorption kinetics was also analysed via in-situ Raman measurements. Since the electrochemical melting starts at potential of -1100 mV vs. Ag/AgCl (3 M KCl) and the ssDNA starts to desorb at -1300 mV vs. Ag/AgCl (3 M KCl), -1250 mV vs. Ag/AgCl (3 M KCl) was chosen for further dsDNA dehybridization. In the last step, SNP detection was accomplished by monitoring the signal decrease with time due to the applied potential. Modified SERS substrates were hybridized with single mismatched target DNA and fully-matched target DNA separately. Potential-assisted DNA melting was monitored via in-situ Raman measurements. The results showed that 60% of the signal from SNP-containing target DNA was lost after 60 s of melting, while only 10% of fully matched target DNA was dehybridized in that time. Furthermore, the reproducibility of the designed sensor was satisfying.

Key words: DNA biosensor, SERS, Langmuir-Blodgett, bipolar electrochemistry, the potential assisted, melting point.

ACKNOWLEDGEMENTS

I would also like to express my deepest thanks to my supervisor Prof. Dr. Handan YAVUZ ALAGÖZ not only for her guidance during my master studies, but also for her friendly attitude, and moral support.

I would like to express my sincere thanks to Prof. Dr. Adil DENİZLİ for his suggestions and guidance throughout my master period.

Also, I would like to express my special appreciation and thanks to Prof. Dr. Wolfgang SCHUHMANN for giving me the possibility to make my master thesis in his group.

I am so deeply indebted to Yasin Uğur KAYRAN for his valuable contribution to my lab performance and important suggestions during my master thesis, likewise for his patient and friendly attitude.

I would like to express my gratitude to Dr. Daliborka Jambrec for her guidance. Whenever I am on the horns of a dilemma about my studies, she enlightened me with her experiences.

Also, I would like to thank my thesis committee members: Assoc. Prof. Dr. Nilay BERELİ, Assist. Prof. Dr. Fatma Yılmaz and Assist. Prof. Dr Ceren Haktanır for their time and interest.

I would like to thank to Vera Eßmann for teaching me how to work bipolar electrochemistry.

I would like to thank all Elan group as they provided a joyful and friendly working environment.

In addition, I would like to thank all of the Biochemistry Research Group for their friendship and cooperation.

I am grateful to my friends Cevahir ATAK and Nesli ÖZKAN for their endless support and friendship.

Above all, I would like to convey my sincere thanks to my family. I deeply appreciate my parents for their understanding and unlimited support.

CONTENTS

	<u>Page</u>
ÖZET	i
ABSTRACT	iii
ACKNOWLEDGEMENTS.....	v
CONTENTS.....	vi
TABLE	viii
FIGURES	ix
SYMBOLS AND ABBREVIATIONS.....	xii
1. INTRODUCTION.....	1
2. GENERAL INFORMATION	2
2.1. Langmuir-Blodgett Films.....	2
2.2. Raman Spectroscopy	6
2.3. Surface Enhanced Raman Spectroscopy (SERS).....	7
2.4. Bipolar Electrochemistry.....	10
2.5. DNA Biosensors	11
2.5.1. Immobilization of DNA probes	13
2.5.2. Determination of DNA Hybridization	14
2.5.2.1. Gravimetric Detection	15
2.5.2.2. Electrochemical Detection	15
2.5.2.2.1. Electrochemical DNA Melting	16
2.5.2.3. Optical Detection	16
3. EXPERIMENTAL.....	18
3.1. Materials.....	18
3.2. Nanovoid Structures.....	19
3.2.1. Electrode Preparation for Nanobeads Deposition	19
3.2.2. Nanobeads Assembly by Means of Langmuir–Blodgett Technique	19
3.2.3. Nanovoids Determination	20
3.2.3.1. Bipolar Electrochemistry Setup	20
3.2.3.2. Modification of the Gold Surface with 4-Nitrothiophenol (NTP)	21
3.2.3.3. SERS Scanning of the Modified Bipolar Electrode	21
3.2.3.4. Determination of Required Potential by Using the BPE.....	21
3.2.4. Electrochemical Setup and Application	21

3.2.4.1. Instrumentation.....	21
3.2.4.2. Electrochemical Gold Deposition.....	22
3.2.5. Removal of Nanobeads.....	22
3.3. DNA Sensor Preparation.....	22
3.3.1. Electrode Cleaning and Characterization.....	22
3.3.2. Probe DNA Immobilization.....	24
3.3.3. Surface Passivation.....	24
3.3.4. Surface Characterization.....	24
3.3.5. DNA Hybridization.....	24
3.3.6. SERS Detection of DNA Hybridization.....	25
3.3.7. Electrochemical DNA Melting.....	25
3.3.8. Investigation of dsDNA Dehybridization Kinetics.....	25
3.3.9. Reproducibility.....	25
4. RESULTS AND DISCUSSION.....	27
4.1. Optimization of the Structure of Gold Nanovoid-Electrodes.....	27
4.1.1. Optimization of Nanobead Size and Gold Thickness.....	27
4.1.2. Optimization of Gold Deposition Procedure.....	31
4.2. Optimization of SERS Parameters.....	35
4.3. DNA Mismatch Analysis by Monitoring DNA Dehybridization Kinetics.....	38
4.3.1. Build-up of the DNA Sensor.....	38
4.3.2. Electrochemically Driven DNA Dehybridization.....	44
4.3.4. Reproducibility.....	47
5. CONCLUSIONS.....	49
REFERENCES.....	51
CURRICULUM VITAE.....	56

TABLE

Page

Table 3.1. The sequences of the employed probe and target oligonucleotides are presented. Cy3 refers the Raman reporter dye Cyanine 3, and (SS)₃ present the dithiol linker attached to the oligonucleotides for surface anchoring.....18

FIGURES

	<u>Page</u>
Figure 2.1. a) Langmuir-Blodgett deposition and b) Langmuir-Schaefer deposition.	2
Figure 2.2. Diagrams on a Wilhelmy plate: a) front view, b) side view. Figure redrawn and adapted from ref. [7]	3
Figure 2.3. Isotherm graph following the formation of LB films.....	5
Figure 2.4. Diagram of Rayleigh and Raman scattering process. Figure redrawn and adapted from ref. [16]	7
Figure 2.5. The wavelength ranges of Au, Ag and Cu for SERS. Figure adapted from ref. [23].....	9
Figure 2.6. Bipolar electrochemistry configuration.....	10
Figure 2.7. Formation of hydrogen bond between a) A-T and b) G-S	12
Figure 2.8. Fragment of a DNA structure.	13
Figure 2.9. Principle of DNA sensor.	15
Figure 3.1. Langmuir–Blodgett Trough.....	20
Figure 3.2. Cyclic voltammogram of a SERS substrate in 0.5 M H ₂ SO ₄ with 25 .. 24 cycles at 100 mV/s scan rate.....	24
Figure 4.1. General principle of the preparation of SSV substrates: 1) template preparation with polymer nanobeads, 2) metal deposition between nanobeads, 3) dissolution of the template.....	27
Figure 4.2. Schematic representation of the fabrication of Au deposit gradients on polymer modified substrates using BPE.....	28
Figure 4.3. SERS spectrum of 4-NTP on a 300 nm diameter nanovoids structured substrate. The accumulation time was 10 s, and the laser power was 1 mW using a 660 nm excitation laser.	29
Figure 4.4. Signal intensities of the N-O stretching band over the bipolar electrode where a) 200 nm diameter, b) 300 nm diameter c) 500 nm diameter d) 600 nm diameter polymer nanobeads were used as templates. Spectra were performed with a 1 mW with a 660 nm excitation laser and the bipolar electrodes were scanned with 100 μm increments.	30
Figure 4.5. SERS spectra of 4-NTP from different sized SSV surfaces. The spectra were recorded with a single 10 s acquisition upon excitation with a 660 nm laser	

and are presented after baseline correction. The incubation time of 4-NTP was 24 h.	31
Figure 4.6. SEM images of the point on SSV substrate (at 1700 μm from cathodic edge of the BE) with the highest SERS intensity.	32
Figure 4.7, a-c. Chronoamperograms presenting the Au deposition by varying the deposition time at a fixed deposition potential [-0.610 V vs Ag/AgCl (3 M KCl)]...	33
Figure 4.8. Comparison of the SERS intensity from adsorbed 4-NTP for cases from the figure 4.7. The error bars indicate the standard deviation from 5 independent measurements.	34
Figure 4.9. SERS spectrum of Cy3 labelled tDNA on 200 nm diameter nanovoids structured substrate. The laser power was 4.4 mW using a 660 nm excitation laser.	35
Figure 4.10. SERS spectra of Cy3-labelled DNA at different power densities of 0.33 mW, 1.58 mW and 4.4 mW, respectively. Comparison of a) Raman signal intensity and b) signal-to-noise ratio.	36
Figure 4.11. SERS spectra of Cy3-labelled DNA using an entrance slit of 100 μm and 1000 μm , respectively. Comparison of a) Raman signal intensity and b) optical resolution.	37
Figure 4.12. Representative SERS spectra of Cy3 labelled DNA for different gratings.	38
Figure 4.13. Representative CVs of a clean gold electrode. Electrochemical cleaning was performed in 0.5 M H_2SO_4 at a scan rate of 100 mV/s.	39
Figure 4.14. Schematic representation of the DNA sensor fabrication using the potential assisted immobilization method.	40
Figure 4.15. Principle of the potential assisted DNA immobilization method where a) application of potential pulses results in b) the observed current-time profile. .	40
Figure 4.16. CV characterization of an Au electrode surface using the 10 mM PB, 20 Mm K_2SO_4 containing 5 mM $\text{K}_3[\text{Fe}(\text{CN})_6]$ and $\text{K}_4[\text{Fe}(\text{CN})_6]$ at a scan rate of 100 mV/s.	41
Figure 4.17. Schematic representation of the target labelled DNA hybridization..	41
Figure 4.18. ssDNA immobilization using the potential assisted method for 1 min, and Cy3-labeled tDNA by incubating for 10 min. a) schematic representation of DNA hybridization b) SERS spectrum, the laser power at 1.58 mW using a 660 nm excitation laser.	42

Figure 4.19. Immobilization of ssDNA (3 min) and Cy3-labelled tDNA with incubation (10 min) a) schematic representation b) SERS spectrum was recorded at a laser power at 1.58 mW using a 660 nm excitation laser and an accumulation time of 10 s.....	43
Figure 4.20. ssDNA immobilization (2 min) and tDNA with Cy3-labelled incubation (10 min) a) scheme presenting the DNA sensor b) the detection of the DNA duplex at the surface of a sphere segment void substrate. The spectra was recorded with 10 s acquisition and a 660 nm excitation laser.	44
Figure 4.21. Schematic representation of the potential melting curve experiment sequence.....	45
Figure 4.22. dsDNA melting curve and ssDNA desorption curve as a function of the applied potential. Experiment was performed in 10 mM PB buffer containing 450 mM K ₂ SO ₄	46
Figure 4.23. DNA dehybridization kinetics of a fully matched and a single mismatched dsDNA. The applied potential was set at -1250 mV vs. Ag/AgCl (3 M KCl) in 10 mM PB buffer containing 450 mM K ₂ SO ₄	47
Figure 4.24. Reproducibility of the developed DNA sensor. The spectrum used is from the Cy3 labelled tDNA and the non-labelled probe DNA.	48

SYMBOLS AND ABBREVIATIONS

Symbols

ρ_p	Material Density
ρ_L	Solution Density
γ	Surface Tension of a Liquid
θ	Contact Angle
g	Gravitational Constant
$\Delta\gamma$	Surface Tension
ΔF	Net Force
π	Surface Pressure Value
Cy3	Dye Cyanine 3

Abbreviations

DNA	Deoxyribonucleic Acid
ssDNA	Single Stranded DNA
SERS	Surface Enhanced Raman Scattering
SSV	Sphere Segment Voids
LB	Langmuir-Blodgett
IR	Infrared Spectroscopy
CARS	Coherent Anti-Stokes Raman Spectroscopy
EM	Electromagnetic Effect
CM	Chemical Effect
LSPR	Localized Surface Plasmon Resonances
BE	Bipolar Electrochemistry
BPE	Bipolar Electrode
QCM	Quartz Crystal Microbalance
SPR	Surface Plasmon Resonance
NTP	Nitrothiophenol
DCM	Dichloromethane
CV	Cyclic Voltammetry
PB	Phosphate Buffer
MCH	Mercaptohexanol

SEM	Scanning Electron Microscopy
dsDNA	Double Strand DNA
pDNA	Probe DNA
pzc	Potential Zero Charge
SNP	Single Nucleotide Polymorphisms

1. INTRODUCTION

Deoxyribonucleic acid (DNA) is unarguably the central molecule of life [1]. Growing demand for genetic information has broadened a range of disciplines and also led to research into the new techniques for genetic analysis. An example of these techniques is a DNA biosensor. The DNA biosensor combines a recognition layer (a single stranded DNA, ssDNA) and a transducer in order to monitor hybridization with a target DNA. The hybridization results from multiple hydrogen bonds generated between base pairs. The hybridization event is converted into a readable signal by the transducer. There are several different readout techniques - electrochemical, optical, and gravimetric approaches.

Concerning sensitivity and simplicity, optical detection methods have provided beneficial opportunities. Surface enhanced Raman scattering (SERS) is an optical detection method that provides enhanced Raman signals due to the presence of plasmonic hot spots [2]. SERS-based DNA sensors are in the spotlight due to the high sensitivity and the specificity of the technique [3]. The mentioned plasmonic hot spots are created on nanostructured surfaces. Different structures have been investigated until now such as nanotriangles, [4] nanorings, [5] spherical nanoshells, two-dimensional gratings, and sphere segment voids (SSV) with respect to their ability to create the electromagnetic enhancement [6]. The main challenge connected with these structures is the reproducibility of the formation of these structures.

In this study, SSV structures are created using Langmuir-Blodgett technique and optimized with respect to the SERS signal enhancement by means of bipolar electrochemistry. The second part of this study is focused on the development of a procedure for dsDNA de-hybridization that will allow distinguishing fully matched dsDNA from single mismatched DNA. The procedure consists of potential-assisted DNA de-hybridization coupled with the detection by in-situ SERS measurements.

2. GENERAL INFORMATION

2.1. Langmuir-Blodgett Films

Langmuir-Blodgett (LB) is a widely used technique for fabrication of thin films employed in many fields [7]. In the first half of the 20th century, Irving Langmuir and Katherine Blodgett developed this technique inspired by the formation of thin films of oil on water surfaces [8]. Afterwards, the method was further developed by many research groups. LB relies on the formation of well-organized self-assembled mono- and multilayers [9].

The working principle of the LB technique is the deposition of a guest sample on a host solid support to form LB films. The water surface in the LB trough is covered by sample molecules. By compressing the LB barriers towards the host solid support dipped in water a desired surface pressure is reached. The solid substrate is slowly pulled out from the solution while simultaneously sample molecules are deposited on its surface, while the pressure is kept constant using the LB barriers [7, 10].

There are two ways of formation of LB films – horizontal and vertical deposition (Figure 2.1). Films obtained by the vertical deposition method are called Langmuir-Schaefer films, while horizontally prepared films are Langmuir-Blodgett films [11].

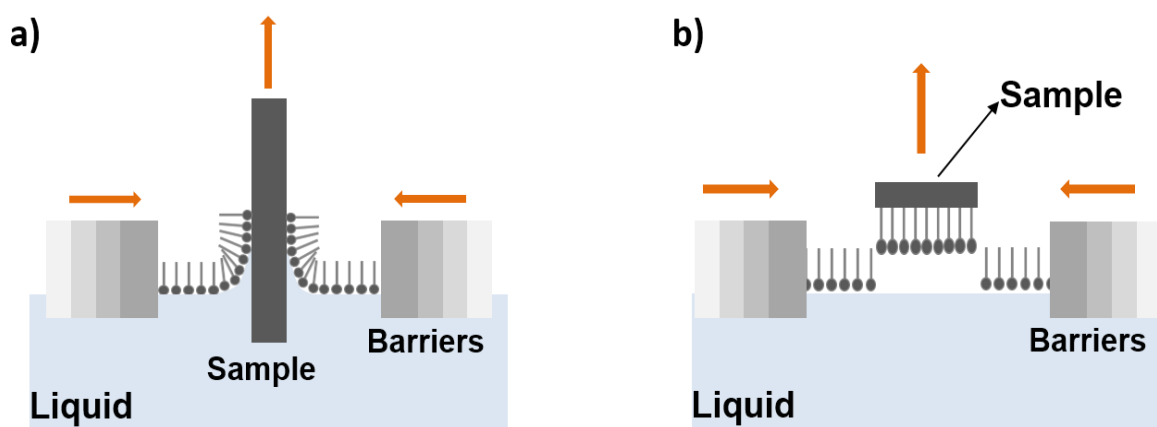


Figure 2.1. a) Langmuir-Blodgett deposition and b) Langmuir-Schaefer deposition.

It is crucial to know properties of the sample used for the formation of LB films because of the hydrophilic and hydrophobic interactions between substrate and substance. Amphiphilic molecules are mostly preferred since they consist of both a hydrophilic part (a head group) such as $-OH$ and $-COOH$ groups, and a hydrophobic part (a tail group) usually consisting of a long alkyl chain [9].

Before the deposition process, sample molecules should be mixed with a volatile solvent and placed on the surface of a sub-phase of the LB trough (water) using a micro-syringe. The advantage of volatile solvents is the ability to evaporate easily after which the remaining sample molecules start spreading on the sub-phase surface. The following step consists of compression of sample molecules with the LB barriers. During this step, the surface pressure is monitored using the Wilhelmy plate method (Figure 2.2) [9]. Namely, a metal plate is immersed in the sub-phase in proximity to the substrate surface (however, not too close to disturb the deposition process). The surface pressure is measured indirectly by measuring the forces acting on the plate during the process, namely gravity, surface tension downward and buoyancy upward. The sensitivity limit of the method is approximately $5 \times 10^{-3} \text{ mN m}^{-1}$ [7].

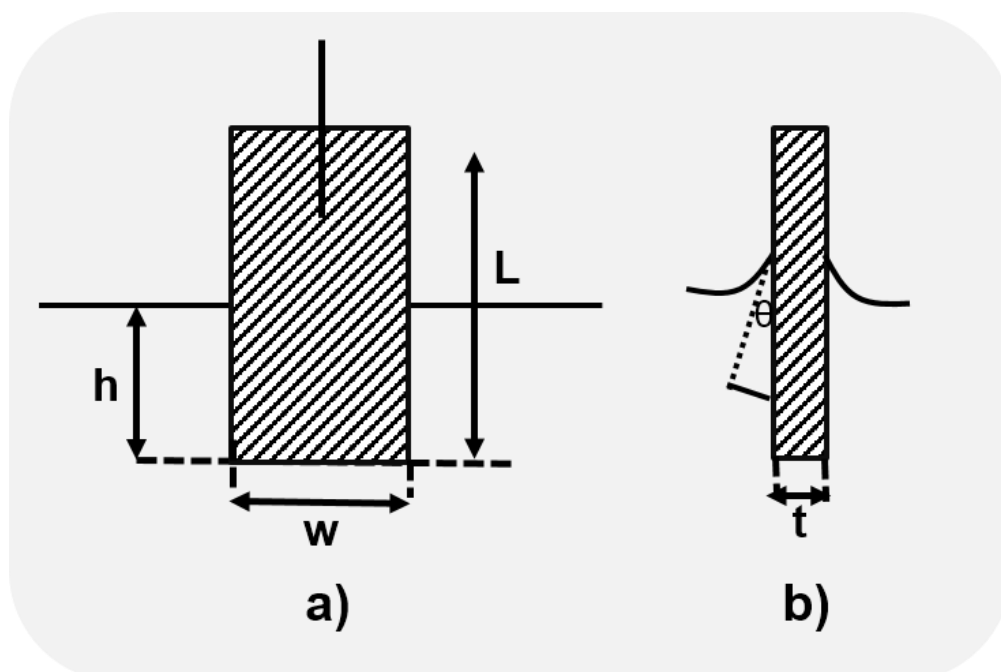


Figure 2.2. Diagrams on a Wilhelmy plate: a) front view, b) side view. Figure redrawn and adapted from ref. [7]

The net downward force can be explained by the following equation:

$$F = \rho_p glwt + 2\gamma(t + w)\cos\theta - \rho_L gtw h \quad (2.1)$$

where ρ_p and ρ_L are the density of a material and of the solution, respectively. γ is the surface tension of a liquid, θ is the contact angle on the solid plate and g refers to the gravitational constant. The contribution of the gravity can be eliminated from the equation by resetting the pressure before the measurement. Furthermore, the contact angle is zero when the plate is completely wetted. So the previous equation becomes:

$$F = 2(t + w)\gamma \quad (2.2)$$

The change in the surface tension ($\Delta\gamma$) depends on the distribution of the sample molecules on the water surface and its change affects the net force (ΔF):

$$\Delta F = 2(t + w)\Delta\gamma \quad (2.3)$$

If the plate is thin enough ($t \ll w$):

$$\Delta\gamma = \frac{\Delta F}{2w} \quad (2.4)$$

Thus, the force change is followed by monitoring the change in the surface tension. For monolayer formation surface pressure can be used as the only parameter in a measurement. Accordingly, the surface pressure value, π , is equal to the reduced pure liquid surface tension caused by the film formation [7]:

$$\pi = -\Delta\gamma \quad (2.5)$$

The last step is to follow the deposition of a monolayer using the surface pressure (π) – area of LB trough (A) isotherm graph. The isotherm follows the stability of a monolayer at the water-air interface [9].

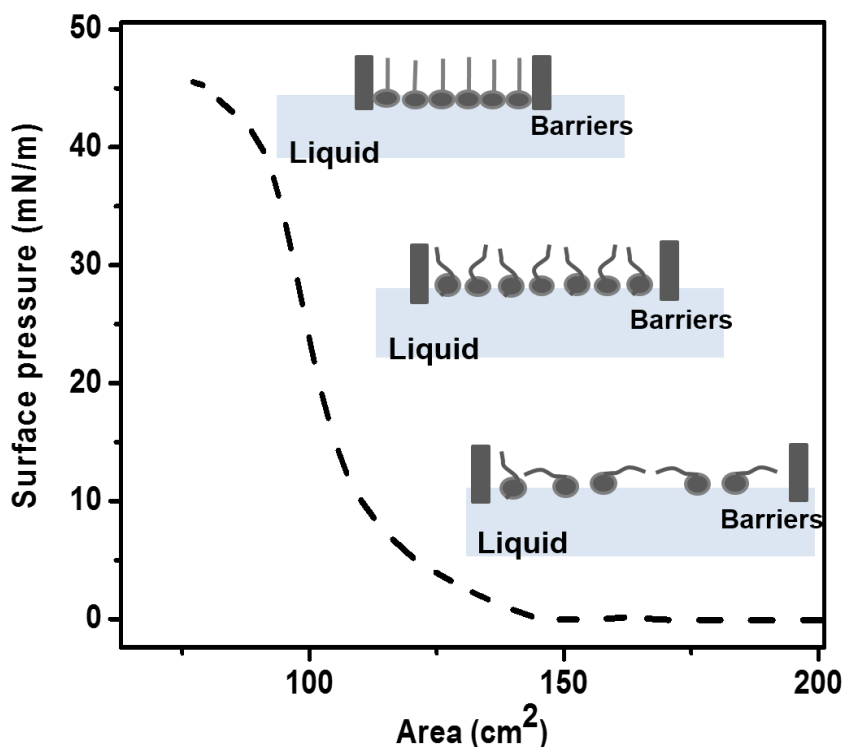


Figure 2.3. Isotherm graph following the formation of LB films.

Figure 2.3 shows three phases of the monolayer formation. The part between 200 cm² and 150 cm² is called “gas phase” due to the low coverage of sample molecules at the water surface. The surface pressure is approximately 0 mN m⁻¹. As barriers proceed to compress, the sample molecules start to interact with each other and the first phase transition is observed from the gas phase to the liquid phase. By further compressing the barriers, the surface area continues decreasing and the transition to a so called solid phase is observed. At the solid phase, molecules are closely packed. If the barriers maintain to move further, some of the molecules may aggregate, collapse or form multilayers at the sub-phase. To form a closely packed monolayer, the surface pressure should be kept at this point and the transfer of the layer to a solid support should be performed in this phase. By repeating this procedure using the same substrate well-organized multilayers may be prepared.

2.2. Raman Spectroscopy

There are various techniques for surface analysis and structural determination. Raman spectroscopy is an important method among them. Raman scattering was discovered by the Indian scientist Sir C. V Raman in 1928. However, after the discovery of the laser, Raman spectroscopy became more powerful, which led to the development of new valuable techniques [12, 13].

Raman spectroscopy belongs to the family of molecular spectroscopies, and it provides information about the structure of analyte molecules due to their vibrational motions. Raman and IR spectroscopy methods are complementary methods [13]. Even though they share some features, the main difference from IR spectroscopy is that in Raman spectroscopy the polarization of the analyte molecule must be changed (tensor quantity) during a Raman active vibration, in contrast to the dipole moment change (vector quantity) [14]. In addition, Raman spectroscopy can be performed in aqueous solutions, while IR spectroscopy is impossible because the O-H bond exhibits a strong absorption for IR radiation. The last difference, concerning the excitation wavelength, is that in IR spectroscopy a monochromatic beam is employed in the infrared region of the electromagnetic spectrum. In Raman spectroscopy, the monochromatic beam or a laser can be in the visible region, the near infrared, or the near ultraviolet range of the electromagnetic spectrum [13, 15].

There are two types of scattering that can be seen in a Raman spectrum, namely Rayleigh scattering and Raman scattering. When the energy of an incident light and scattered light are at the same level, the scattered light is called Rayleigh scattering or elastic scattering. On the other hand, Raman scattering includes two different level-states. If the energy of the incident light is higher than the energy of the scattered light, this scattering is called anti-Stokes. In the opposite case, if the energy of an incident light is lower than the energy of scattered light, it is called Stokes (Figure 2.4) [16].

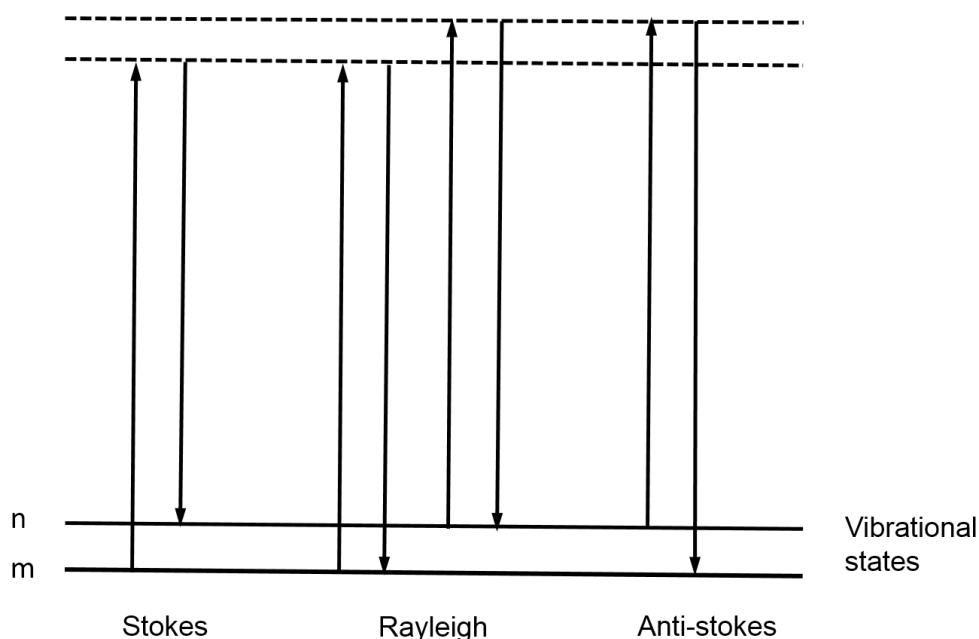


Figure 2.4. Diagram of Rayleigh and Raman scattering process. Figure redrawn and adapted from ref. [16]

In order to increase the range of applications and the limited sensitivity of Raman spectroscopy several techniques were developed such as resonance Raman spectroscopy, coherent anti-stokes Raman spectroscopy (CARS), and surface enhanced Raman spectroscopy (SERS). Among them, the SERS method is the most popular one due to the incredibly high sensitivity.

2.3. Surface Enhanced Raman Spectroscopy (SERS)

Surface Enhanced Raman Spectroscopy (SERS) has been widely used as a detection method with an enhanced Raman signal. The reported enhancement factor of SERS is around 10^4 - 10^6 , and it can be increased up to 10^8 - 10^{14} [12]. Compared to Raman spectroscopy, SERS enables to increase the sensitivity of the Raman signals and provide potentially single molecule detection. The SERS technique has been used widely in many fields, including trace analysis, detection of biomolecules, catalysis, the characterization of modified electrodes etc. [13]. The technique provides a very sensitive detection by means of SERS substrates. The high sensitivity of the SERS technique broadens the use of Raman spectroscopy in the biochemistry field, for example for the detection of DNA (deoxyribonucleic acid) hybridization [17].

In 1974, Fleischman et al. were the first group who observed the enhancement of the Raman signal from pyridine molecules, which was adsorbed onto an electrochemically roughened silver surface [18]. Subsequently, Jeanmaire et al. and Creighton et al. reported independently that the reason of the high Raman scattering is the effect of surface enhancement. They proposed two mechanisms to explain the signal enhancement – the electromagnetic effect (EM), which occurs due to the rough metal surface and the chemical effect (CM), due to interactions between adsorbed molecules and the metal surface. These mechanisms are still widely accepted to explain the SERS effect [15].

The first mechanism of SERS enhancement is based on the formation of an electric field provided by a roughened metal surface. The process of electromagnetic enhancement includes the following stages: at first, an incident light excites the localized surface plasmon on the metal surface. The localized surface plasmon can be described as the collective oscillation of the confined electrons of a conductor. The localized plasmons can create an electrical field at the near surface region [19]; secondly, analyte molecules near the surface of the metal substrate will be polarized by the electric field. Enhanced electrical field in the vicinity of the metal structures will enhance the Raman signals [19–21].

The magnitude of electromagnetic enhancement depends on several factors, such as the electric properties of the metal substrate, the incident light frequency, the distance between molecules and the surface and the surface morphology [15]. Due to the presence of localized surface plasmons rough structures provide a great enhancement compared to smooth surfaces. The localized surface plasmon properties are extremely dependent on surface properties of the metal structures, hence, size, shape and structure of the substrate are crucial to acquire the strongest SERS signal. In general, electromagnetic enhancement provides enhancements of the Raman signals up to 10^4 to 10^7 times [21].

Chemical enhancement is also called a signal enhancement since the charge transfer is based on bond formation between analyte molecules and a metal surface. The molecular orbital of the adsorbate molecules are broadened into resonances because of the interactions with electrons in the conduction band. In this way, the molecular polarizability of molecules is increased in a particular way.

Consequently, the major factors of chemical enhancement are the surface, which increases the molecular polarizability, and the chemical nature of the analyte molecules [16]. The crucial point to get strong Raman scattering is the distance between analyte molecule and the SERS substrate. When the analyte molecules adsorb closely to the SERS substrate, the SERS spectrum may show stronger Raman peaks. An important point of SERS enhancement is the metal nanostructure which is used to support the propagation of the surface plasmons. Also, the wavelength of the surface plasmon has a major role in obtaining the SERS enhancement. Hence, the wavelength and the amplitude of the plasmon propagation at the structure surface are responsible for the intensity of SERS.

Researchers have focused mostly on using Au, Ag, and Cu metals to fabricate nanostructures due to their optical properties [22]. Au and Ag substrates are preferred in comparison to Cu substrates due to the fact that they are air stable materials. The three metals have localized surface plasmon resonances (LSPR) which cover most of the visible and near-infrared wavelength range (Figure 2.5) [23].

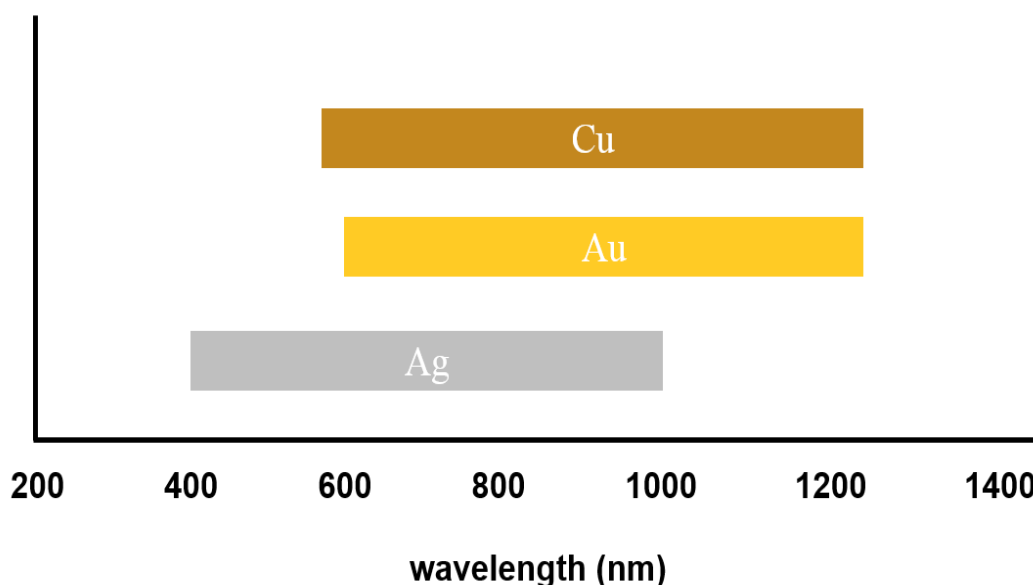


Figure 2.5. The wavelength ranges of Au, Ag and Cu for SERS. Figure adapted from ref. [23]

Most commonly, SERS substrates are prepared via colloidal particle arrays [24], metal grating structures [25] and roughened electrodes [26]. The SERS substrate with colloidal nanoparticles provide a high surface enhancement. However, the main problem of the method is the lack of regularity and reproducibility [27]. Therefore, researchers have reported a variety of approaches to overcome the reproducibility problem; such as the Langmuir-Blodgett (LB) method [28], lithography and imprint methods. Bartlett and co-workers demonstrated the fabrication of SERS substrates using metal nano-cavities fabricated by an electrochemical deposition method. Initially, they coated the metal substrate with polystyrene spheres to prepare a template. Afterwards, a gold electrodeposition procedure was applied to the template to fabricate well-ordered macro-porous films [29]. Furthermore, they showed that the size of nano-cavities has a significant influence on the SERS enhancement [30].

2.4. Bipolar Electrochemistry

Bipolar electrochemistry (BE) is an electrochemical method also known as wireless electrochemistry. BE is based on an electrical field generation by applying a potential difference between two feeder electrodes [31]. BE does not require physical connection between a bipolar electrode (BPE) and a power supply. Another interesting feature of BE is that the oxidation and reduction reactions can arise simultaneously at the opposite poles of the BPE [32].

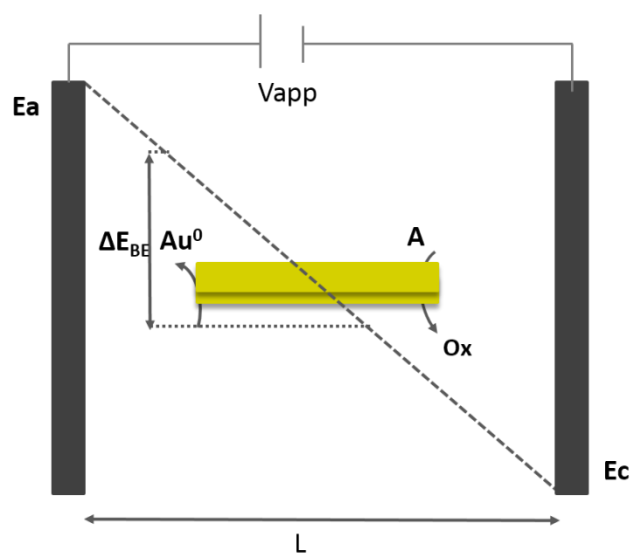


Figure 2.6. Bipolar electrochemistry configuration.

In the BE configuration, the BPE should be located between two feeder electrodes. Feeder electrodes are connected to a power supply. During the current flow through the feeder electrodes, a potential gradient is generated at the BPE due to the electrical field drop in the electrolyte, as illustrated in Figure 2.6 [31].

$$\epsilon = \frac{V_{appl}}{L} = \frac{E_a - E_c}{L} \quad (2.6)$$

Feeder electrodes are positioned at a distance L and d is the length of the BPE. A potential difference $E_{appl} = E_a - E_c$ is created by applying a potential to the feeder electrodes. The potential E_{appl} drops linearly in solution from E_a to E_c if the distortion of the electric field by faradic current at the feeder electrodes is negligible. Therefore the potential difference between the substrate and the solution becomes the driving force for the bipolar electrochemical reactions [33]. Bipolar electrochemistry has been employed in research areas such as surface modification, electroanalytics and biosensors, as well as material science. Additionally, compositional grading of materials was explored using BE [34, 35].

2.5. DNA Biosensors

Biosensors are analytical devices based on highly specific biorecognition events to detect target analyte molecules. A biosensor consists of a biological recognition element and a transducer. Transducers convert the interaction between the recognition element and the target molecule into an electrical signal. Biosensors can be classified into two groups, bioaffinity and biocatalytic devices. Bioaffinity devices depend on the selective binding between the target analyte and a surface-confined complementary binding partner. On the other hand, biocatalytic devices depend on immobilized biological recognition elements, which recognize and catalytically convert the target substrate [36]. So far, biosensors consist of enzyme sensors, DNA sensors, immune-sensors and microbial sensors [1].

DNA biosensors are used in vital applications such as gene analysis, sequencing, DNA diagnostic, detection of biological warfare agents and forensic applications to provide a high-throughput analysis [2]. Deoxyribonucleic acid (DNA), known as the

key biomolecule in human life, consists of two polynucleotide chains called DNA strands. These DNA strands are linked together through the formation of hydrogen bonds between their nucleobases. A DNA strand consists of a chain of subunits known as nucleotides. Nucleotides are composed of a deoxyribose sugar attached to a phosphate group that forms a backbone of a DNA chain and a nitrogen-containing nucleobase. The nucleobases are divided into two groups, purines and pyrimidines. Purines are adenine (A) and guanine (G), and pyrimidines are cytosine (C) and thymine (T). Based on the Watson-Crick base pairing model, adenine forms two hydrogen bonds with thymine while cytosine and guanine are connected with three hydrogen bonds (Figure 2.7) [37].

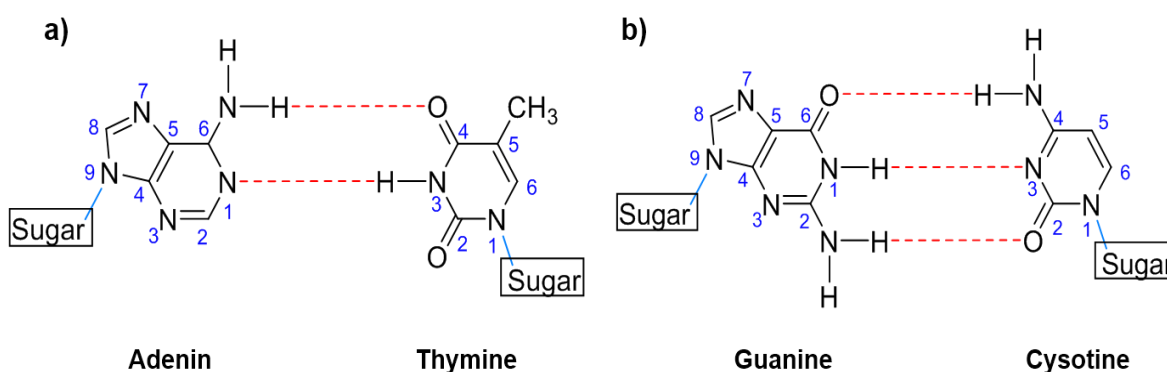


Figure 2.7. Formation of hydrogen bond between a) A-T and b) G-S.

The nucleotides are linked together via phosphodiester bonds between 5' and 3' C atoms of the deoxyribose to create a single-stranded DNA (ssDNA) (Figure 2.8) [37]. DNA sensors rely on hybridization-based recognition processes between a probe DNA and its complementary target DNA [2]. In order to design a DNA sensor, several factors should be considered such as the immobilization of a DNA probe, the functionality of the surface-bound probes, and the reproducibility of the attachment chemistry [38].

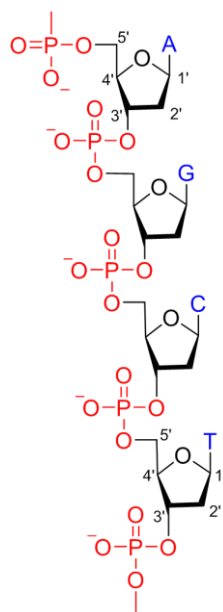


Figure 2.8. Fragment of a DNA structure.

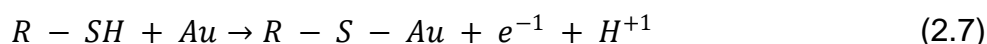
2.5.1. Immobilization of DNA probes

Immobilization is the attachment of probe molecules to a solid surface using a specific chemical reaction. This is a crucial step in creating a DNA biosensor. The control of the immobilization step is important to obtain high reactivity, orientation, accessibility, stability of the surface-confined DNA probe and removal of non-specific binding. DNA probes are considered as short oligonucleotides that hybridize with a particular target DNA chain. There are several methods to achieve the immobilization of probe DNA such as physical adsorption, covalent immobilization, and streptavidin-biotin immobilization.

Physical adsorption is a straightforward method for the immobilization of ssDNA. It is based on the ionic interaction between the negatively charged phosphate backbone of the DNA and positive charges on the surface. Electrostatic interactions between the probe molecules and the electrode surface can be increased by surface modifications. The physical adsorption approach presents a simple, fast and direct immobilization without using linked molecules. However, this method suffers from some drawbacks such as a random orientation, poor reproducibility, and weak attachment of DNA molecules on the electrode surface. The DNA probes may be removed by environmental factors such as pH value,

temperature, ionic strength or by some solvents, because of the weak attachment of ssDNA to the surface [38].

Covalent attachment is a widely used method for probe DNA immobilization since it provides strong binding. Besides this, good long term stability is one of the main advantages of this method. However, prior to covalent attachment an activation of a surface or an adsorbent needs to be performed and the fact that the binding is irreversible presents the main disadvantage of the approach. Gold-thiol (Au-S) binding is often considered as a subgroup of covalent binding, even though the mechanism of this reaction is still under debate in the scientific community. There are many mechanisms proposing the nature of this bond, most of them suggesting chemisorption and physisorption. The major advantage of this approach is the mobility of already attached molecules on the surface to form energetically favoured packing. This interaction is widely used to attach thiolated DNA to Au electrodes due to the strong affinity of thiol groups to the metallic surfaces [2, 38].



Due to the high affinity of biotin towards avidin, this interaction is used in many applications. Biotin is a small molecule, while avidin is a tetrameric protein, which has four identical binding units for biotin. Regarding its application in a production of DNA sensors, the method suffers from some limitations such as multiple step immobilization that increases the production time and cost. Another limitation is the unspecific adsorption of avidin on the surface [2].

2.5.2. Determination of DNA Hybridization

The probe DNA grafted on the electrode surface is exposed to the solution containing target DNA molecules complementary to the sequence of the immobilized probe DNA. The recognition process is converted into a measurable signal, which can distinguish the hybridization. The detection of a signal can be obtained via different detection techniques, where the most commonly used are electrochemical, optical or gravimetric detection schemes (Figure 2.9) [2].

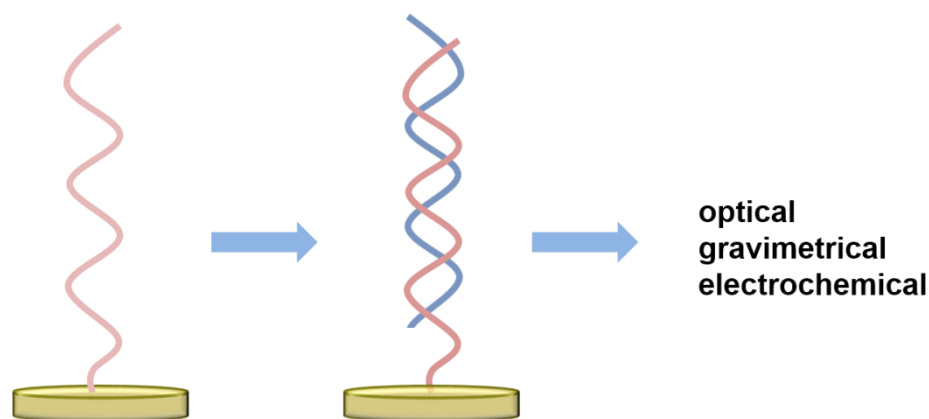


Figure 2.9. Principle of DNA sensor.

2.5.2.1. Gravimetric Detection

Quartz crystal microbalance (QCM) is the most widely used gravimetric technique that measures the mass change upon hybridization of the immobilized probe DNA with the target DNA from solution. QCM is an extremely sensitive technique that provides a real-time monitoring of the hybridization event. A QCM based DNA sensing system contains an oscillating crystal and an immobilized probe DNA layer on its surface. When the hybridization reaction occurs at the surface of the crystal, the oscillation frequency starts to decrease. The level of the decrease depends on the mass change at the electrode surface. Therefore a fully-matched target DNA, non-complimentary target DNA or mismatched target DNA can be distinguished [36, 39].

2.5.2.2. Electrochemical Detection

In general, electrochemical detection methods for the hybridization of DNA are based on monitoring the current response under controlled applied potential conditions. Strategies used for the electrochemical detection of the hybridization process can be grouped into direct and indirect electrochemical detection of the target DNA. Direct detection is based on the reduction and/or oxidation of DNA bases at a mercury drop electrode. The oxidation of guanine is the easiest among the nucleobases. Palecek and co-workers pioneered this approach [40]. Indirect hybridization detection is readily performed using redox mediators, labelled target

DNA, by a sandwich type assay, where a third labelled sequence hybridizes with an overhang of the target DNA, or via non-covalently interacting indicators [39].

2.5.2.2.1. Electrochemical DNA Melting

Dehybridization of DNA is the separation of the double helix into two ssDNA strands. Hydrogen bonds between complementary bases can be broken down using certain driving forces. Some of those stimulants are pH value, temperature, ionic strength, and potential [41]. In 1974, the first study of electrochemically driven DNA dehybridization was performed [42, 43]. Denaturation of dsDNA at negative potentials was done at a mercury drop electrode. Since then many mechanisms were proposed to understand the electrochemical DNA melting process. One of them suggests the repulsion of the negatively charged DNA backbone at a negative applied potential. Recently, Bartlett and co-workers employed electrochemically induced DNA denaturation to distinguish DNA mutations in the gene responsible for cystic fibrosis and to detect short tandem repeats as used in forensics.

Gold sphere segment void (SSV) substrates were used to enhance Raman signals, and Au-S chemistry was used for the immobilization of probe DNA. The Raman signal decreased due to the increase of the negative potential, suggesting a more efficient dehybridization. The melting potential was defined in relation to the melting temperature as the potential at which 50% of dsDNA is dehybridized [44].

2.5.2.3. Optical Detection

Krull and co-workers created the first optical DNA biosensor with an extremely low detection limit, using ethidium bromide as DNA intercalator [45]. Fluorescence based optical biosensors have a high sensitivity, about 10^7 molecules/cm². Besides fluorescence methods, surface plasmon resonance (SPR), surface enhanced Raman scattering (SERS), colorimetric or chemiluminescent measurements have also been employed as detection methods.

The SPR system requires a thin metal coated prism. When the incident light is shone on the prism with a particular angle, the intensity of the reflected light decreases. The particular angle is called the resonance angle, and it is extremely sensitive to changes at the metal surface. Changes at the metal/air interface caused by DNA hybridization invoke a shift in the resonance angle. Therefore, DNA hybridization can be detected by means of SPR in a label-free manner. Expensive and complicated instrumentation is the main limitation of the method [2].

SERS-based detection has been widely investigated for direct or indirect detection of DNA, proteins and cellular components owing to their unique Raman signal. The use of Raman active dyes significantly increases sensitivity. They are used as labels or intercalators in order to create a clear, specific and strong signal [46, 47]. Indirect detection of DNA via SERS can be classified into two approaches: using metal nanoparticles or by using SERS substrates. Harpster and co-workers performed an indirect DNA detection of target DNA, via methylene blue (Raman active dye) acting as an intercalator, using a single Au nanoparticle [48]. Graham *et al.* employed a SERS substrate to detect DNA hybridization, where Ag nanoparticle-aggregate substrates provided the signal enhancement. Hybridized tDNA placed between Ag nanoparticles was used as a linker to merge nanoparticles [46].

3. EXPERIMENTAL

3.1. Materials

Colloidal polystyrene nanobead suspensions (10 % (w/w) in H₂O) with various diameters, Φ 200 nm, 300 nm, 500 nm, and 600 nm were supplied by Thermo Fischer Scientific (USA). Ethanol (C₂H₆O), cysteamine (C₂H₇NS), 6-mercapto-1-hexanol, K₃[Fe(CN)₆], K₄[Fe(CN)₆], and hydrogen peroxide (H₂O₂) were purchased from Sigma-Aldrich Chemie (Germany). Sulfuric acid (H₂SO₄) was obtained from J. T. Baker. K₂SO₄, KH₂PO₄, and K₂HPO₄ were purchased from VWR International (Germany). Gold plating solutions (ECF60 and E3) were bought from Metalor Technologies (United Kingdom). 4 - Nitrothiophenol (NTP) was supplied from Fluka (CH). 200 nm thick Au evaporated Silicon wafers were provided from the Department of Physical Chemistry II of the Ruhr-Universität Bochum (Germany). All aqueous solutions were prepared from double distilled ultra-pure water ($\rho < 18 \text{ m}\Omega \text{ cm}^{-1}$). All oligonucleotides were bought from FRIZ Biochem (Germany) and are listed in Table 3.1.

Table 3.1. The sequences of the employed probe and target oligonucleotides are presented. Cy3 refers the Raman reporter dye Cyanine 3, and (SS)₃ present the dithiol linker attached to the oligonucleotides for surface anchoring.

Code	Sequence
P1	5' TGC GGA TAA CAC AGT CAC CT TTTTTTTT (SS) ₃
P1_Cy3	5' Cy3-TGC GGA TAA CAC AGT CAC CT TTTTTTTT (SS) ₃
T1-Cy3	5' (Cy3) - AGG TGA CTG TGT TAT CCG CA
T1-Cy3-1MM	5' (Cy3) - AGG TGA CTG T <u>A</u> T TAT CCG CA

3.2. Nanovoid Structures

3.2.1. Electrode Preparation for Nanobeads Deposition

The Au wafer was cut to the desired size using a glass cutter. Au electrodes were immersed in a fresh piranha solution [H_2SO_4 : H_2O_2 , 3:1 (v/v)] to clean organic residues from the electrodes surface. The clean electrode was incubated in 5 mM ethanolic solution of cysteamine for 24 h to increase the hydrophilicity of the wafer surface.

3.2.2. Nanobeads Assembly by Means of Langmuir–Blodgett Technique

The used Langmuir–Blodgett trough was from Biolin Scientific (Sweden). The main parts of a LB device are a trough and two moveable barriers. Components of the employed setup are shown in Figure 3.1. All Langmuir-Blodgett experiments were performed in a glass cage in order to avoid contaminations. The trough and the barriers were rinsed with distilled water and ethanol, respectively, before each experiment. The Pt Wilhelmy plate was heated in advance with a torch to clean it. After the cleaning step, the plate was connected to an electronic balance. Distilled water was employed as the sub-phase for all experiments. The sub-phase surface was cleaned with a Pasteur pipette to ensure the cleanliness of the water surface. Subsequently, a robotic hand dipped an Au wafer into the cleaned sub-phase. Afterwards, 210 μl polymer nanobeads suspension (2:1 v/v, ethanol: stock nanobeads suspension) was added to the sub-phase surface by using two microscope slides. The glass slides were located at the edges of the trough. Hence, the nanobeads were gradually dispersed to the water-air interface. The surface pressure was adjusted to 0 mN m^{-1} before the experiments. The mobile barriers were compressed at a rate of 10 $\mu\text{m min}^{-1}$ in order to provide a closely packed nanobeads film. The surface pressure was slowly increased following the isotherm graph. In other words, a well-organized monolayer film was initiated to form at the water-air interface. Then, the moveable barriers were stopped when the surface pressure reached a saturation point. While the Au wafer was retracting from the sub-phase, the surface pressure was kept constant. Thus, a monolayer of nanobeads was transferred to the solid substrate.

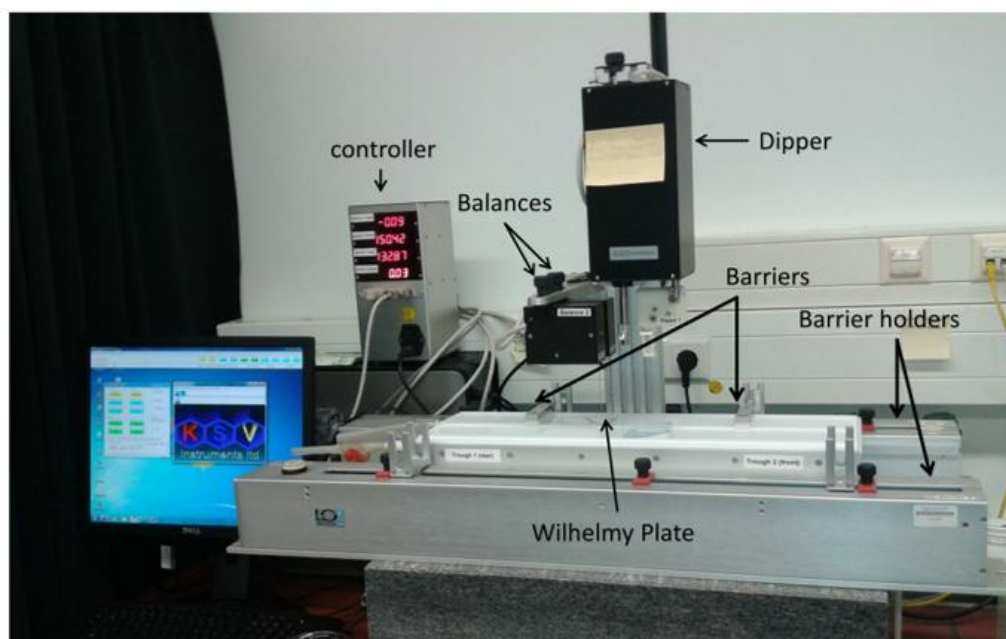


Figure 3.1. Langmuir–Blodgett Trough

3.2.3. Nanovoids Determination

3.2.3.1. Bipolar Electrochemistry Setup

A homemade bipolar electrochemistry cell was employed for all BE experiments [31]. The setup consisted of two feeder electrodes and a bipolar electrode. Two carbon rods (>160 mm, Ø 6.2 mm) were used as feeder electrodes. In order to obtain clean carbon surfaces, the carbon rods were polished with a polishing paper and sonicated in distilled water for 5 min. The feeder electrodes were fixed at the edge of the cell. A nanobeads film deposited Au wafer was used as the bipolar electrode and positioned in the middle of the cell. The cell was filled with a freshly prepared Au plating solution [200:1 (v/v), ECF60/E3]. The applied potential was calculated using equation 4.1. When the potential was started to be applied by using a high-voltage potentiostat (AMETEK, USA), the colour of the BE surface was gradually changed from the middle of the BE to the cathodic edge. The applied potential was stopped, when the colour of the cathodic part was turned to dark brownish. When the experiment was stopped, the deposition time was determined and the deposition time was 120 s.

3.2.3.2. Modification of the Gold Surface with 4-Nitrothiophenol (NTP)

4-NTP was used as a Raman indicator. The electrodes were soaked in 5 mM 4-NTP solution overnight.

3.2.3.3. SERS Scanning of the Modified Bipolar Electrode

SERS analyses of modified bipolar electrodes were performed using a Jobin-Yvon IHR55 Raman (Horiba, Japan) setup with a monochromatic laser ($\lambda=660$ nm). Raman spectra were recorded in the wavelength range from 300 cm^{-1} to 1700 cm^{-1} . The accumulation time was 10 s, and a 60 X microscope objective (Olympus, Japan) was used. The bipolar electrodes were scanned with $100\text{ }\mu\text{m}$ increments.

3.2.3.4. Determination of Required Potential by Using the BPE

After the SERS scanning experiment, the position with the highest Raman intensity was determined. The applied potential at the found position was measured with a reference electrode. The potential was -0.610 mV vs. Ag/AgCl (3 M KCl).

3.2.4. Electrochemical Setup and Application

3.2.4.1. Instrumentation

A three electrode system was used for all electrochemical measurements, except the bipolar electrochemistry experiments. A nanostructured Au electrode was used as working electrode. The counter electrode was a platinum wire (Goodfellow, Germany) and the reference electrode was a homemade Ag/AgCl (3 M KCl) or Pb/PbF₂ (5 M KF) electrode. All electrochemical measurements were performed with a potentiostat (PGSTAT302N; Metrohm-Autolab, The Netherlands).

The homemade Pb/PbF₂/ 5 M KF reference electrode was fabricated according to a procedure by La Mantia et al. [49]. A Pb wire was polished using a P400 abrasive paper and then rinsed with distilled water. The wire was connected to a copper wire, and the connection was isolated by a shrinking tube. PbF₂ deposition was performed onto the Pb wire in a 0.5 M NaF solution by cyclic voltammetry. The deposition was performed within 20 cycles at a scan rate of 20 mV/s and a potential range of 200 mV to -890 mV vs. Ag/AgCl (3 M KCl). In the first cycle, the

potential was decreased to a more negative potential. By this, the deposition was improved due to the removal of the oxide layer from the Pb wire surface. A chronoamperometry protocol was followed to increase the stability of the PbF_2 film: a potential of 200 mV vs. Ag/AgCl (3 M KCl) was applied for 2 h. In order to fabricate the reference electrode, a glass cover was prepared with a Pasteur pipet. A ceramic frit was placed at the tip of Pasteur pipette, and the pipette was filled with 5 M KF solution. Eventually, the deposited wire was placed in 5 M KF, and sealed with a shrinking tube. The electrode potential was checked before each experiment, and it was around -620 mV vs. Ag/AgCl (3 M KCl).

3.2.4.2. Electrochemical Gold Deposition

An Au electrodeposition procedure was employed to generate Au nanostructures. A commercially available Au plating solution was used for the electrodeposition. Before the deposition at a constant potential, cathodic potential pulses were employed to create Au nuclei at the electrode surface. According to the pulse profile, high cathodic potentials (-1.4 V vs. Ag/AgCl) were applied for 10 times with a very short pulse duration (50 ms). After each pulse, the electrodes were kept at OCP for 1 s. The nuclei formation was followed by Au electrodeposition at a constant potential [-0.610 V vs. Ag/AgCl (3 M KCl)].

3.2.5. Removal of Nanobeads

The polymer nanobeads were dissolved in dichloromethane (DCM). In order to provide complete removal of the polymer nanobeads, the electrodes were sonicated in DCM for 3 min. After the removal procedure, the electrodes were rinsed thoroughly with distilled water and dried under argon atmosphere.

3.3. DNA Sensor Preparation

3.3.1. Electrode Cleaning and Characterization

In order to provide a clean SERS substrate, chemical and electrochemical cleaning procedures were employed. The chemical cleaning was performed in Piranha solution. The SERS substrate was soaked in Piranha solution

[H₂SO₄:H₂O₂, 3:1 (v/v)] to clean from organic residues at the substrate surface. Electrochemical cleaning was performed by employing a cyclic voltammetry procedure in 0.5 M H₂SO₄. A potential range between 0 V to 1.6 V vs. Ag/AgCl (3 M KCl) was swept for 25 times at 100 mV/s scan rate. The roughness factor was calculated using the following equations and always kept around 1.4 according to [50].

$$R = \frac{A_{real}}{A_g} \quad (3.1)$$

$$A_g = r^2\pi \quad (3.2)$$

$$A_{real} = \frac{Q_{exp}}{Q_{theor}} \quad (3.3)$$

$$Q_{exp} = \frac{peak\ area}{V} \quad (3.4)$$

A_g is the geometrical surface area of the electrode, A_{real} is the real surface area of the electrode. Q_{theor} is 482 $\mu\text{C}/\text{cm}^2$ and Q_{exp} is the charge included in the gold oxide reduction. V is the scan rate of the measurement and peak area is the area which is under the reduction peak from the CV measurement (Figure 3.2).

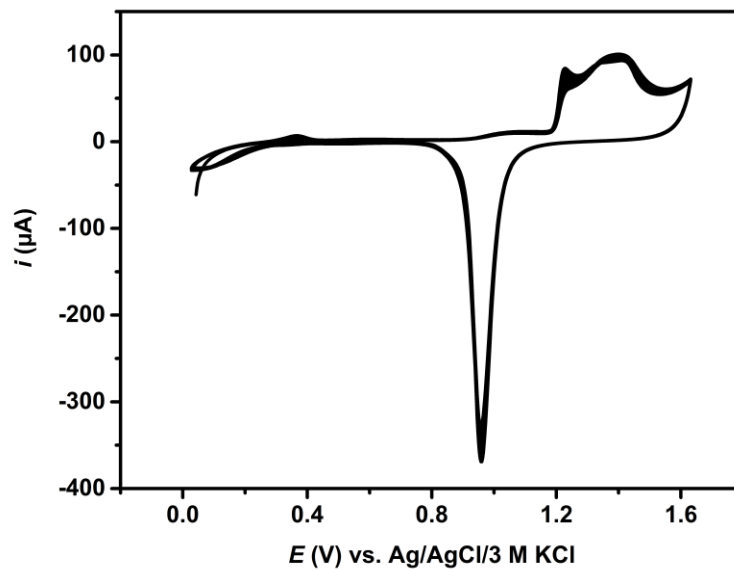


Figure 3.2. Cyclic voltammogram of a SERS substrate in 0.5 M H₂SO₄ with 25 cycles at 100 mV/s scan rate.

3.3.2. Probe DNA Immobilization

DNA immobilization was performed by using the potential-assisted method [51]. A pulse profile of 0.5 V to -0.2 V vs. Ag/AgCl (3 M KCl) was applied to the cleaned electrodes with a 10 ms pulse duration. The pulses were applied for 2 min in 1 μM ssDNA solution containing 10 mM PB, 450 mM K₂SO₄. In order to provide a stable attachment, thiolated ssDNA molecules were employed. After the surface modification, the electrode was rinsed with 10 mM PB, 450 mM K₂SO₄ to remove the unspecific attachments from the electrode surface. In order to investigate the probe DNA desorption kinetics, 5' Cy3 labelled ssDNA molecules were immobilized following the above-mentioned procedure.

3.3.3. Surface Passivation

Pinholes at the electrode surface were covered with mercaptohexanol (MCH). The above mentioned potential-assisted pulse immobilization method was similarly employed for MCH immobilization. A pulse profile was applied to the electrodes for 1 min in 1 mM MCH in 10 mM PB, 20 mM K₂SO₄. After surface modification, the electrodes were rinsed with ethanol and water respectively [52].

3.3.4. Surface Characterization

Electrode surface characterization was achieved via CV measurements. Before each immobilization step, CV measurements were performed in 5 mM K₃[Fe(CN)₆] and K₄[Fe(CN)₆] containing 10 mM PB and 20 mM K₂SO₄. A potential range from -0.1 V to 0.5 V vs. Ag/AgCl (3 M KCl) was swept at a scan rate of 0.1 V/s.

3.3.5. DNA Hybridization

The probe ssDNA immobilized electrodes were incubated in 1 μM Cy3 labelled target DNA solution (in 10 mM PB, 450 mM K₂SO₄) for 10 min at room temperature. After hybridization, the electrodes surfaces were thoroughly rinsed with the same buffer solution to remove unspecific attachments.

3.3.6. SERS Detection of DNA Hybridization

SERS measurements were performed using a homemade in-situ Raman cell. An immersible 60 X microscope objective was used to focus to the electrode surface, and a laser with 660 nm wavelength with 1.58 mW power density was used for excitation. The accumulation time was 20 s, and the repetition was 2 s for each spectrum. The Raman spectra were collected in the wavelength range from 300 cm^{-1} to 1700 cm^{-1} . The front entrance was at 1000 μm and a 600 grooves/mm grating was preferred. In situ Raman measurements were performed in 10 mM PB, 450 mM K_2SO_4 .

3.3.7. Electrochemical DNA Melting

The applied potential ramp was started from -800 mV vs. Ag/AgCl (3 M KCl) and increased till -1700 mV vs. Ag/AgCl (3 M KCl). The increment of the potential ramp was 50 mV. Each potential was applied for 20 s, and after the each potential application a SERS spectrum was collected. The melting potential was about -1300 mV vs. Ag/AgCl (3 M KCl). In order to keep the probe DNA at the electrode surface, a potential of -1250 mV vs. Ag/AgCl (3 M KCl) was chosen as the DNA dehybridization potential.

3.3.8. Investigation of dsDNA Dehybridization Kinetics

In order to initiate DNA dehybridization the chosen potential of -1250 mV vs. Ag/AgCl (3 M KCl) was applied to the dsDNA modified electrodes for 60 s. After each potential application, a SERS spectrum was collected. The intensity of the ring stretching vibration at 1595 cm^{-1} was followed to monitor DNA dehybridization.

3.3.9. Reproducibility

After 4 min potential application, the electrode was incubated in 1 μM target DNA solution for re-hybridization. In order to investigate the reproducibility of the sensor, a potential of -1250 mV vs. Ag/AgCl (3 M KCl) was applied to the

electrode for 5 min, and the decrease in the SERS signal intensity was observed. The procedure was repeated 2 times.

4. RESULTS AND DISCUSSION

4.1. Optimization of the Structure of Gold Nanovoid-Electrodes

4.1.1. Optimization of Nanobead Size and Gold Thickness

Surface enhanced Raman scattering (SERS) is a popular technique for DNA sensor development studies due to the high sensitivity of the method. Since the SERS signal crucially depends on the surface topography, well-designed nanostructured surfaces are the vital point for sensitivity of SERS measurements. Therefore, one of the main goals of my thesis was to create an optimal procedure for fabrication of reproducible SERS substrates that lead to high SERS signals.

Sphere segment void (SSV) structures were selected as suitable SERS substrates due to their high reproducibility, homogeneity of the obtained substrates and the simplicity of the preparation procedure [26]. Fabrication of SSV surfaces was performed on Au deposited silicon wafers in three steps: template preparation with polymer nanobeads, metal deposition between nanobeads and dissolution of the template (Figure 4.1). The first step was performed using a Langmuir-Blodgett technique and the second step was accomplished via electrochemical gold deposition using bipolar electrochemistry or chronoamperometry. As the last step, the electrodes were rinsed with dichloromethane to dissolve the polymer nanobeads.

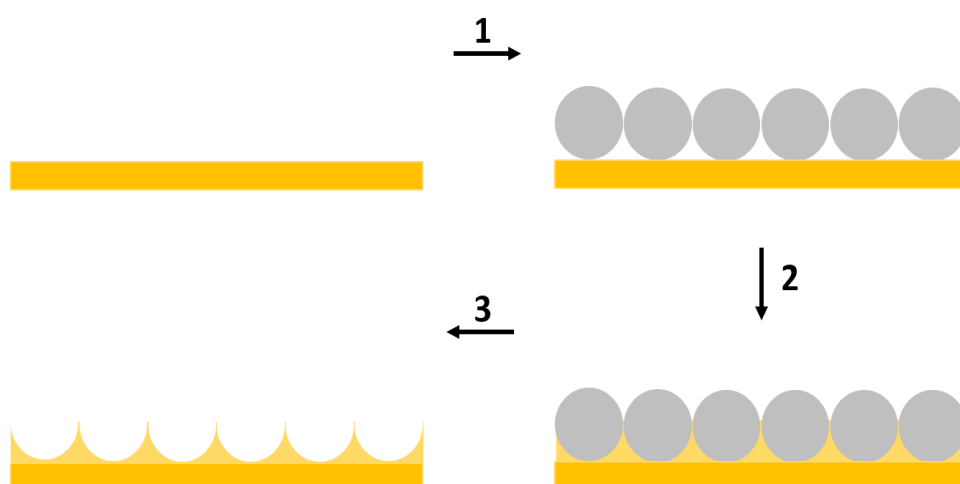


Figure 4.1. General principle of the preparation of SSV substrates: 1) template preparation with polymer nanobeads, 2) metal deposition between nanobeads, 3) dissolution of the template.

To optimize the SSV substrate morphology and obtain the highest Raman intensity various polymer sizes and thicknesses of deposited gold were investigated. Initially, gold substrates were compactly covered with polymer beads, each using a different size of beads (ranging from 200 to 600 nm in diameter). Afterwards, BPE technique was used to produce a gradient of a Au deposit and in this way allow a very efficient and fast investigation of two parameters on the SERS signal – polymer bead size and the potential intensity (Figure 4.2). Due to the principle of BPE, different positions of the BP electrode experience a different potential. Therefore, regions with a low potential result in a thin Au deposition layer since the driving force for the reduction of Au ions from the solution is low, while regions with high potential are covered with a thicker Au deposit.

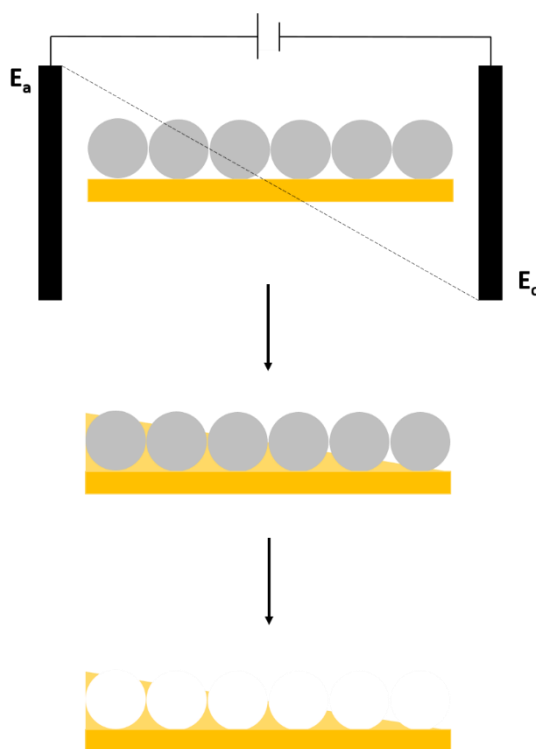


Figure 4.2. Schematic representation of the fabrication of Au deposit gradients on polymer modified substrates using BPE.

Polymer-modified Au wafers were used as bipolar electrodes and positioned in the Au plating solution. The applied potential was calculated from the dependence on the length of the bipolar electrodes.

$$\frac{\Delta E_{BE}}{I_{BE}} = \frac{V_{feeder}}{d_{feeder}} \quad (4.1)$$

In equation 4.1, ΔE_{BE} refers to the potential drop across the BE and the length of electrodes is presented as I_{BE} . V_{feeder} refers to the applied potential between the feeder electrodes, and d_{feeder} is the distance between the feeder electrodes. The distance between feeder electrodes was 150 mm, while the potential across the BE was 3 V. After 120 s, a gradual colour change along the BE surface was observed. Therefore this time was used for the following experiments of electrochemical gold deposition.

To investigate the influence of the surface morphology of the created SSV substrates on the SERS signal, polymer beads were removed from the surface as previously explained and the substrates were modified with a 4-nitrothiophenol (4-NTP) monolayer as SERS active compound followed by the measurement of the SERS signal [31].

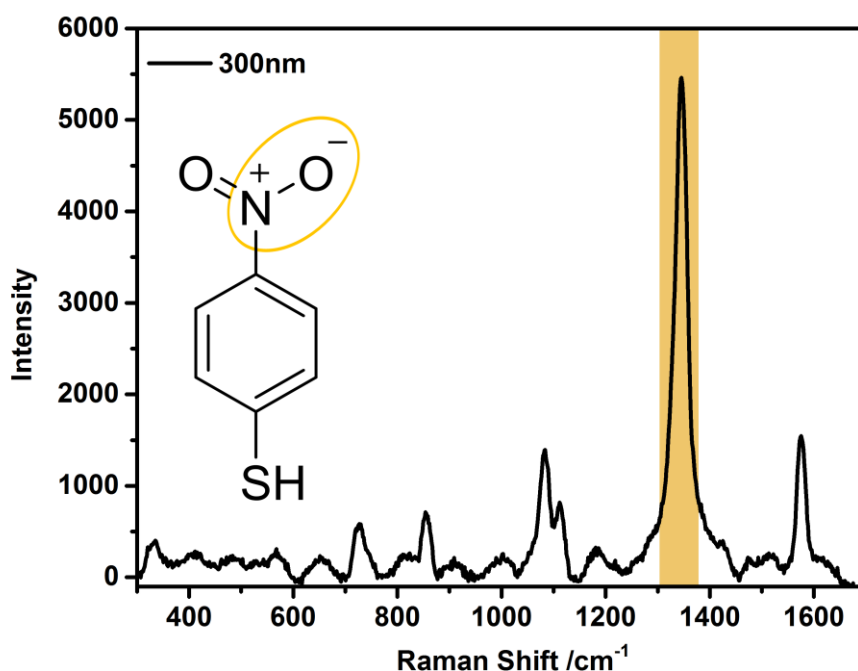


Figure 4.3. SERS spectrum of 4-NTP on a 300 nm diameter nanovoids structured substrate. The accumulation time was 10 s, and the laser power was 1 mW using a 660 nm excitation laser.

Figure 4.3 shows a SERS spectrum of 4-NTP measured on the SSV substrate previously modified with 300 nm diameter nanobeads. The highest peak can be observed at 1345 cm^{-1} , which is characteristic for N—O stretching band [53].

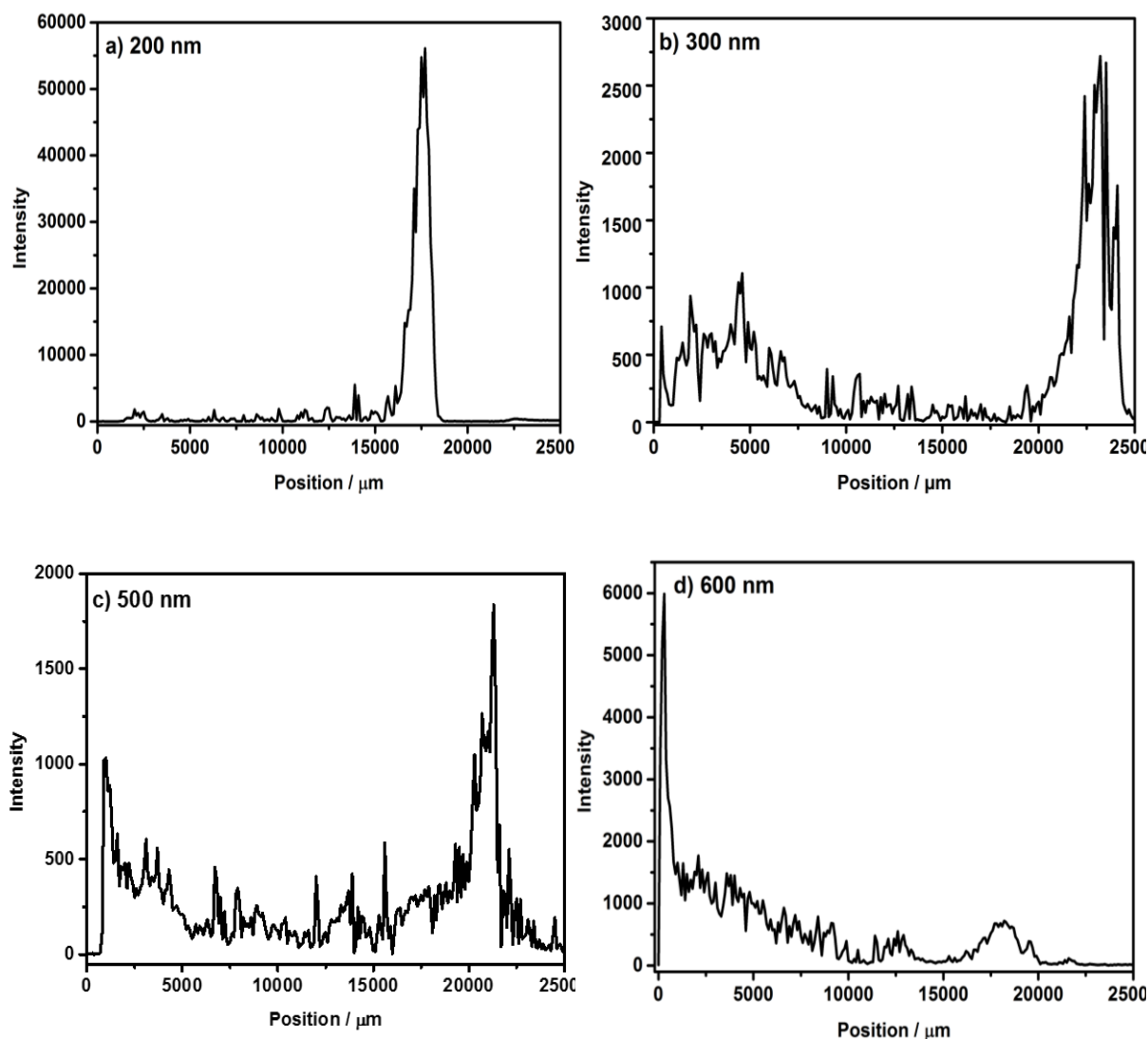


Figure 4.4. Signal intensities of the N-O stretching band over the bipolar electrode where a) 200 nm diameter, b) 300 nm diameter c) 500 nm diameter d) 600 nm diameter polymer nanobeads were used as templates. Spectra were performed with a 1 mW with a 660 nm excitation laser and the bipolar electrodes were scanned with 100 μm increments.

Fabricated BE electrodes were scanned with a Raman super head with an increment of 100 μm . The intensity of the N—O stretching band was extracted from each spectrum and plotted versus the position on the BE (Figure 4.4, a-d) in order to find the highest signal intensity region in dependence on the surface

structure and applied potential. Comparing all substrates it can be observed that a SSV substrate prepared with 200 nm diameter polymer beads provides the highest SERS signal enhancement (Figure 4.5). Thus, for further optimization substrates were prepared exclusively using 200 nm diameter nanobeads.

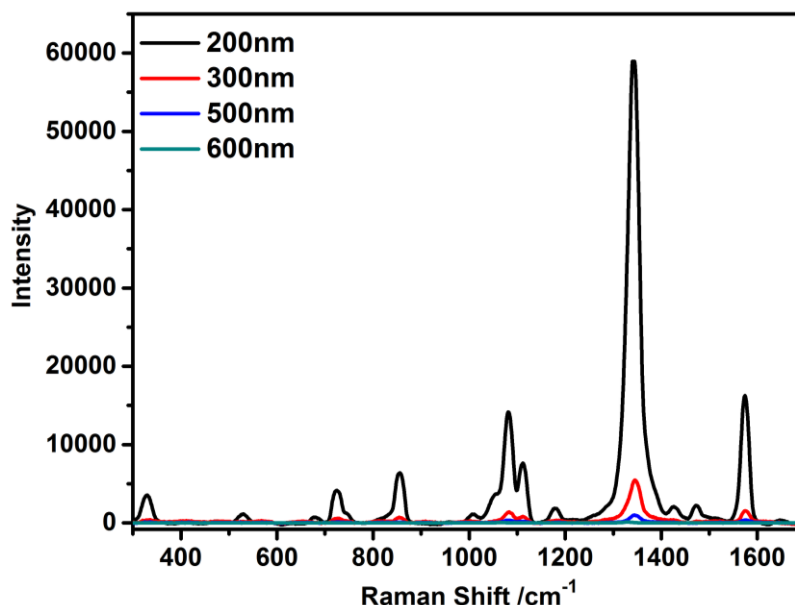


Figure 4.5. SERS spectra of 4-NTP from different sized SSV surfaces. The spectra were recorded with a single 10 s acquisition upon excitation with a 660 nm laser and are presented after baseline correction. The incubation time of 4-NTP was 24 h.

4.1.2. Optimization of Gold Deposition Procedure

In order to find an optimal Au thickness, the strongest peak intensity region was selected from the Figure 4.4, a (17700 μm from the cathodic end of the BE). The required potential was measured in another bipolar electrode experiment. A Ag/AgCl (3 M KCl) reference electrode was positioned at the defined spot and the potential difference was measured between the bipolar electrode and the reference electrode. The determined potential was -0.610 V vs. Ag/AgCl (3 M). Figure 4.6 presents the scanning electron microscopy (SEM) picture showing the morphology of the substrate in this point after the selected time.

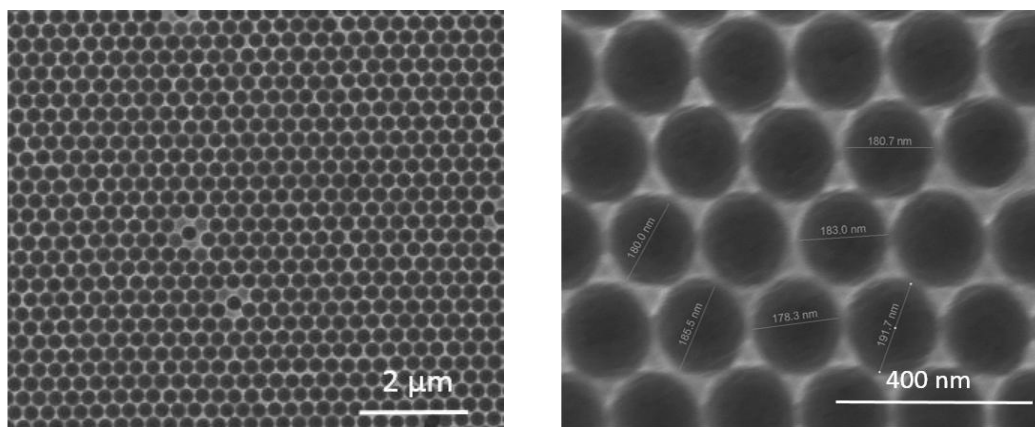


Figure 4.6. SEM images of the point on SSV substrate (at 1700 μm from cathodic edge of the BE) with the highest SERS intensity.

The defined potential was employed to fabricate SSV surfaces by using chronoamperometry. Polymer nanobeads (200 nm diameter) modified Au wafers were used as working electrodes. The potential was kept constant and the deposition time was varied. Figure 4.7, a-c explains the change of the morphology with the time of the deposition. It is generally observed that the surface morphology is rather controlled by the shape of the current-time curve than by the deposition time itself. Depending on many parameters (such as the quality of the modification of the electrode with polymer beads and the cleanliness of the electrode and the deposition solution) the deposition time needed to obtain favourable surface morphology differs between electrodes. However, the shape of the current-time curve is directly connected with the surface morphology. Namely, in the beginning of the deposition nuclei formation is observed and due to this also an initial increase in the current as a result of the increase in the real surface area is seen. Once the Au layer starts growing between the polymer beads the current starts decreasing due to the decrease in the real surface area. This occurs until the point where the polymer beads “touch” each other (Figure 4.7, a). After this point the current increases again since the Au deposit exposes a bigger surface. When the curve again reaches the current maximum the Au deposition layer almost covers the complete polymer beads (Figure 4.7, b). Further deposition causes further increase in the layer thickness. When polymer beads are almost covered current does not significantly change anymore (Figure 4.7, c).

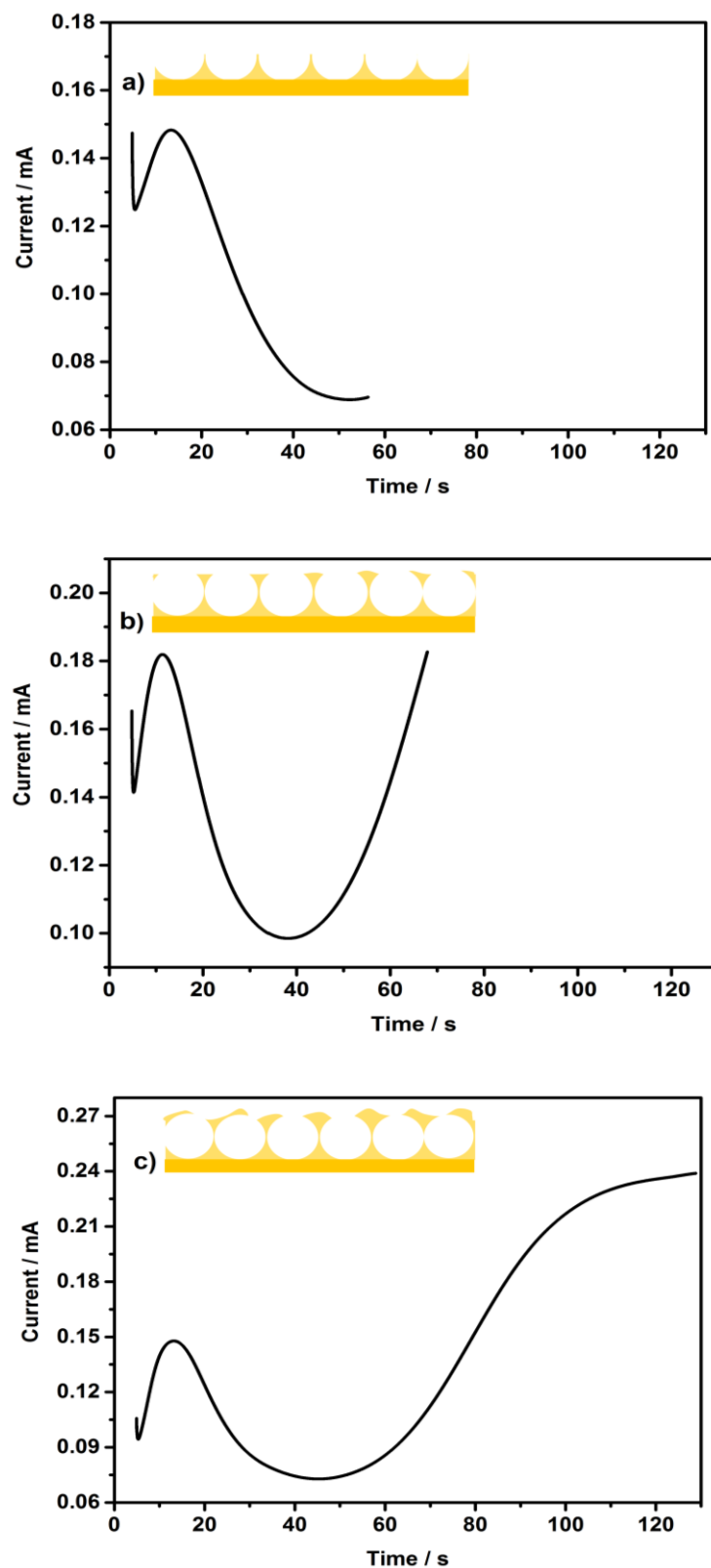


Figure 4.7, a-c. Chronoamperograms presenting the Au deposition by varying the deposition time at a fixed deposition potential [-0.610 V vs Ag/AgCl (3 M KCl)].

These electrodes were further investigated with SERS in order to verify which current-time curve shape is preferable for SERS measurements. After an overnight incubation in 4-NTP, SERS spectra were collected. Five spectra were collected from each electrode to investigate the homogeneity of the surfaces (Figure 4.8). It was observed that the highest SERS signal originates from the surface obtained in the experiment from the figure 4.7, b.

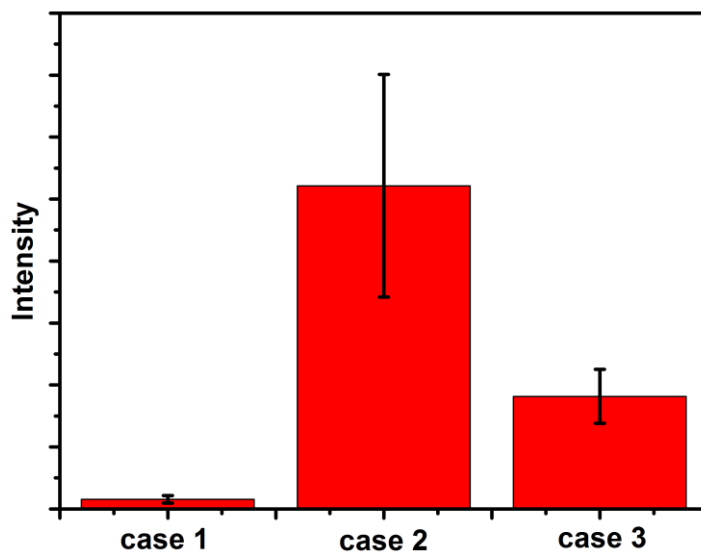


Figure 4.8. Comparison of the SERS intensity from adsorbed 4-NTP for cases from the figure 4.7. The error bars indicate the standard deviation from 5 independent measurements.

Thanks to previous experiments optimal parameters for the preparation of SERS substrates, such as the deposition potential and the best size of nanobeads, are obtained that are used in further experiments. Furthermore, the observation that the shape of the current-time curve is more important than the deposition time itself is an important point for the reproducibility in preparation of SERS substrates. In further experiments, Au deposition was performed until the second maximum in the current is reached. The potential of -0.610 V vs Ag/AgCl (3 M KCl) was used in all further experiments.

4.2. Optimization of SERS Parameters

In order to maximize SERS signals and increase the sensitivity parameters such as the laser power density, slit entrance and gratings were optimized using Cyanine 3 (Cy3)-labelled target DNA, which was later employed in DNA detection experiments. Cy3 is a fluorescent dye that belongs to the synthetic polymethine dyes of the cyanine family. Figure 4.9 shows its characteristic Raman peaks. The band at 1595 cm^{-1} attributes to the C=N chromophore stretch vibration [54]

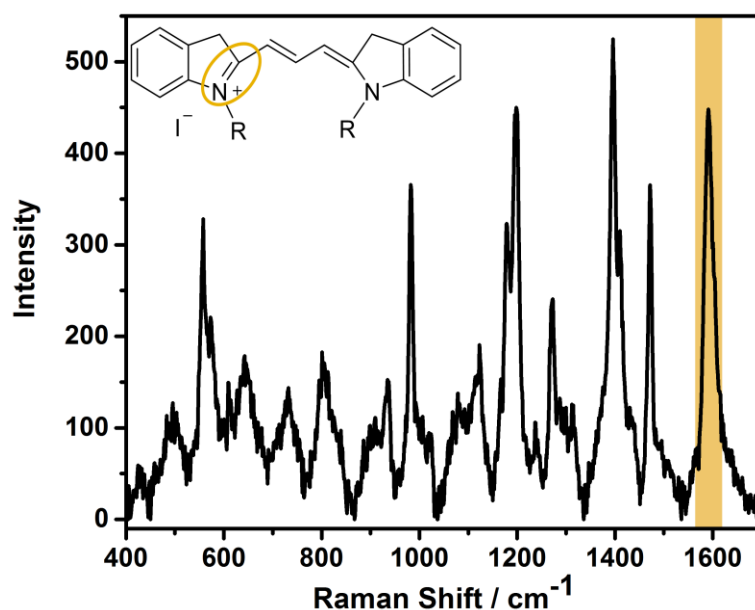


Figure 4.9. SERS spectrum of Cy3 labelled tDNA on 200 nm diameter nanovoids structured substrate. The laser power was 4.4 mW using a 660 nm excitation laser.

The laser power density is directly proportional to the intensity of Raman signal. The higher the power density is, the higher is the intensity of the obtained peaks (Figure 4.10, a). On the other hand, it has to be considered that the DNA structure is sensitive to high laser power density. By increasing the laser power SERS signals increase, and the signal-to-noise ratio decreases (Figure 4.10, b). Even though the laser power of 4.4 mW shows the highest signal, 1.58 mW was preferred for the further experiments because of the stability of the DNA.

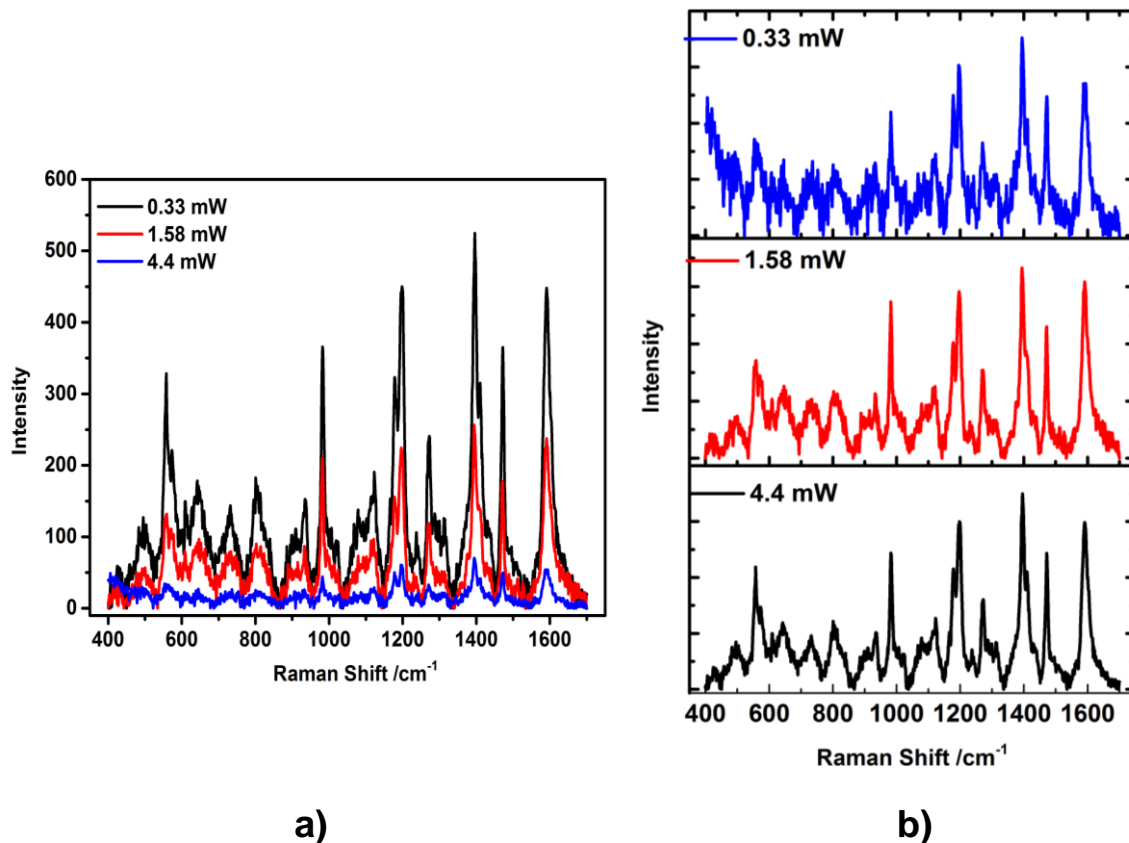


Figure 4.10. SERS spectra of Cy3-labelled DNA at different power densities of 0.33 mW, 1.58 mW and 4.4 mW, respectively. Comparison of a) Raman signal intensity and b) signal-to-noise ratio.

Another crucial parameter is the entrance slit through which the scattered Raman light enters the optical bench; the entrance slit controls the angle of light. Thus, the slit may affect the Raman signal intensity and optical resolution. Since an entrance slit of 1000 μm gives better resolution in comparison to an entrance slit of 100 μm (Figure 4.11, a-b) this value was used in further experiments.

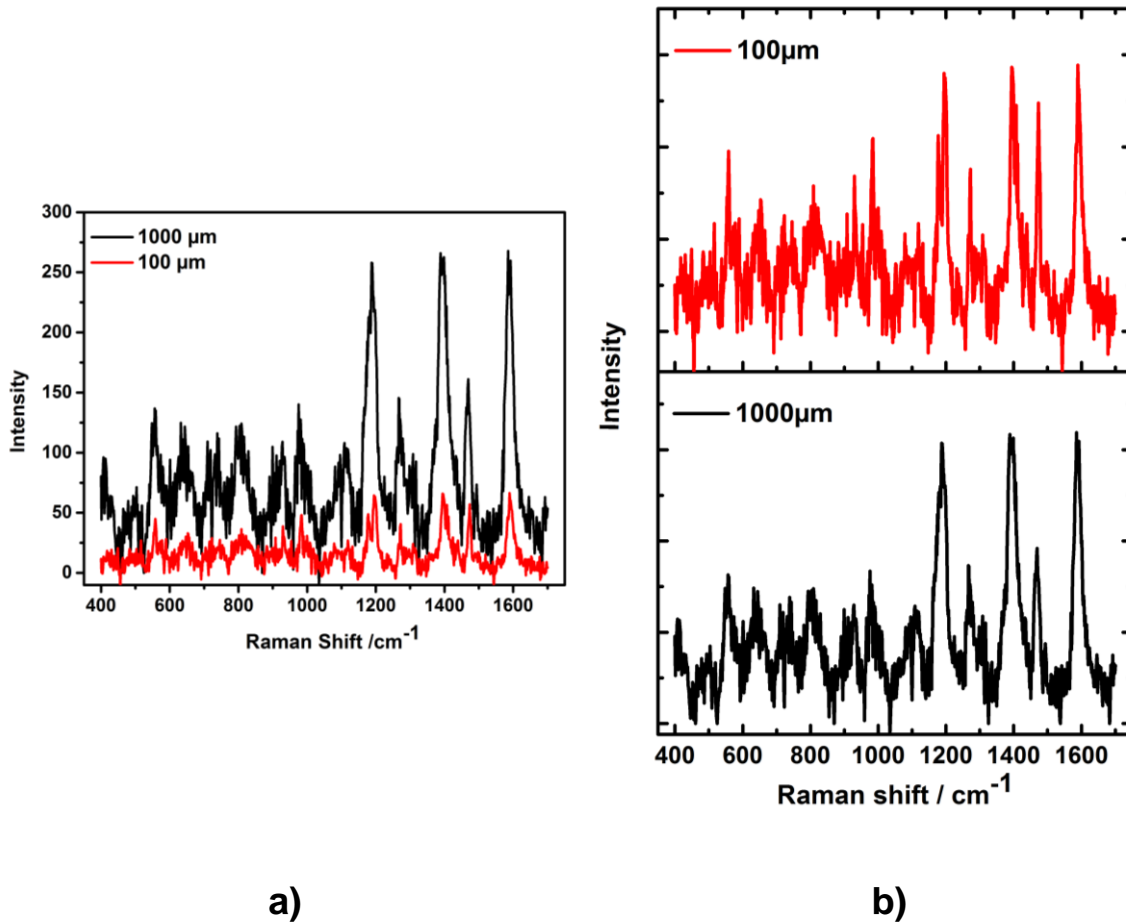


Figure 4.11. SERS spectra of Cy3-labelled DNA using an entrance slit of 100 μm and 1000 μm , respectively. Comparison of a) Raman signal intensity and b) optical resolution.

The effect of the diffraction grating was also investigated to determine the wavelength range and also partially the optical resolution. Despite the peak separation increases by using a grating with a higher amount of grooves the intensity of the peaks decreases (Figure 4.12). Moreover, the required time to collect a spectrum increases with higher grating. Therefore 600 grooves/mm was selected for the further experiments.

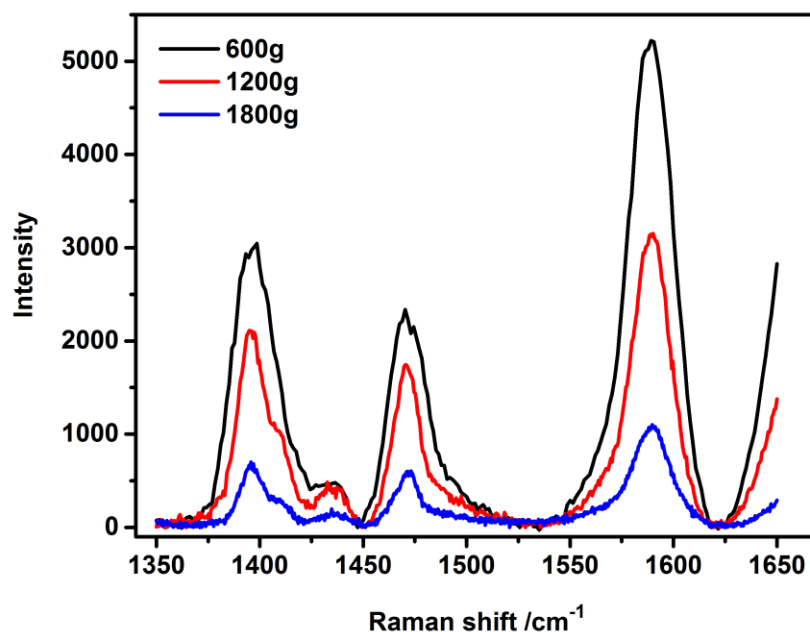


Figure 4.12. Representative SERS spectra of Cy3 labelled DNA for different gratings.

4.3. DNA Mismatch Analysis by Monitoring DNA Dehybridization Kinetics

Sensitive and selective analysis of DNA sequences is vital for the diagnosis of numerous genetic conditions and identification of specific mutations in DNA. A way to detect mutations is by dehybridization, i.e. the separation of the double helix into two single-stranded DNA strands. It is triggered by a change in parameters such as temperature [3] pH value [55] or by application of a certain potential [44]. The aim of this thesis was to design an electrochemical approach for reproducible dehybridization of dsDNA that can distinguish fully matched DNA from single nucleotide polymorphism (target DNA with a single mismatch). An important point that needs to be addressed for DNA dehybridization supported by potential application is the stability of pDNA film on the electrode surface.

4.3.1. Build-up of the DNA Sensor

At the beginning of the fabrication of a DNA biosensor, cleaning of the surface is essential to eliminate any contamination. Therefore, chemical and electrochemical cleaning procedures were employed to the SSV electrodes. Optimized SSV surfaces were used for the preparation of DNA biosensors. Surfaces were initially

cleaned with a fresh Piranha solution, followed by an electrochemical cleaning via CV in H_2SO_4 until stable voltammograms were obtained (Figure 4.13).

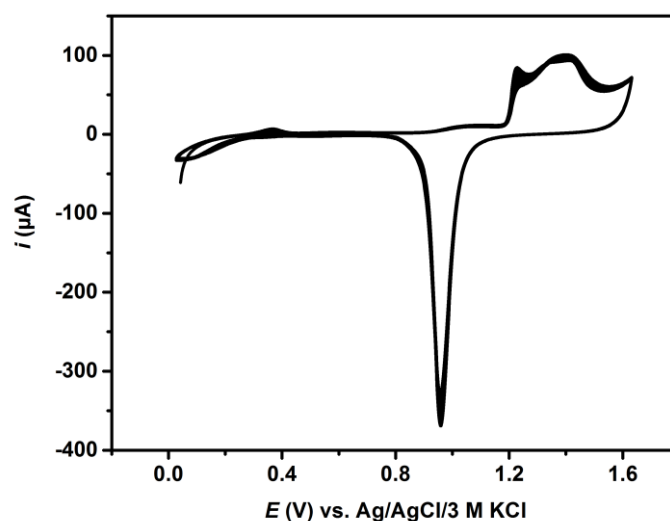


Figure 4.13. Representative CVs of a clean gold electrode. Electrochemical cleaning was performed in 0.5 M H_2SO_4 at a scan rate of 100 mV/s.

After the cleaning step, the DNA-based biosensor was fabricated employing a potential-assisted immobilization method used for both initial DNA immobilization and the further passivation of the surface with MCH (Figure 4.14). Compared to the standard incubation immobilization method using Au-S chemistry, the recently developed potential-assisted immobilization method is much more efficient and at the same time more reproducible [51]. It is based on switching between positive and negative potentials relative to the potential zero charge (pzc) during the surface modification (Figure 4.15). Stirring of ions in the vicinity of the surface is achieved by this and it brings along molecules within the affected layer. Since the immobilization acceleration is a result of ion stirring and not attraction or repulsion of molecules in the solution, this method is equally efficient for both DNA and thiols as charged and uncharged molecules [52].



Figure 4.14. Schematic representation of the DNA sensor fabrication using the potential assisted immobilization method.

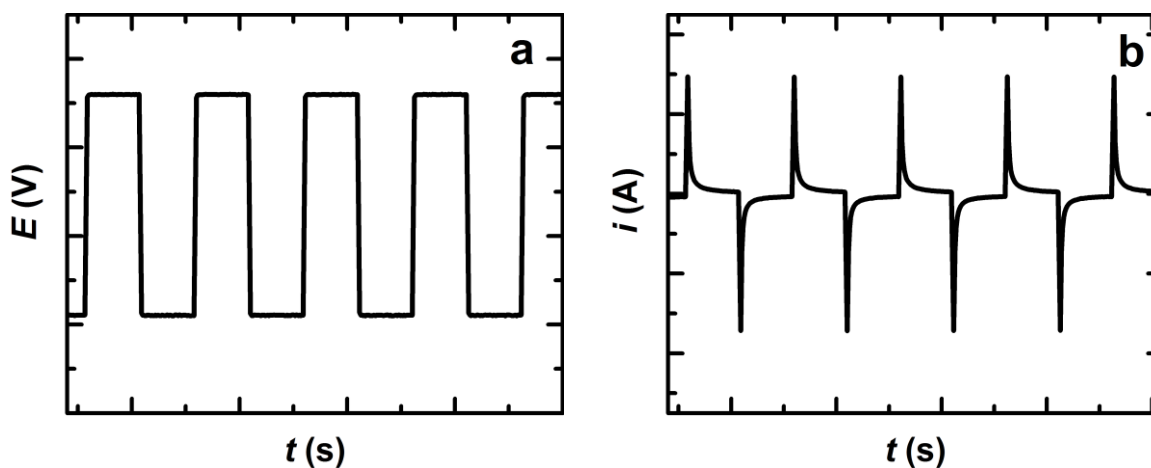


Figure 4.15. Principle of the potential assisted DNA immobilization method where a) application of potential pulses results in b) the observed current-time profile.

The purpose of using the MCH is to avoid the unspecific attachment at the electrode surface. Thus, MCH was employed to cover empty spaces on the SSV surface. Apart from surface passivation, MCH may increase the hybridization efficiency by forcing ssDNA molecules to obtain a more upright orientation [52].

Before the each modification step, the SSV electrode surface was characterized by means of CV in a ferro/ferricyanide solution as a redox probe. By this, the quality of the surface modification was verified during the whole process.

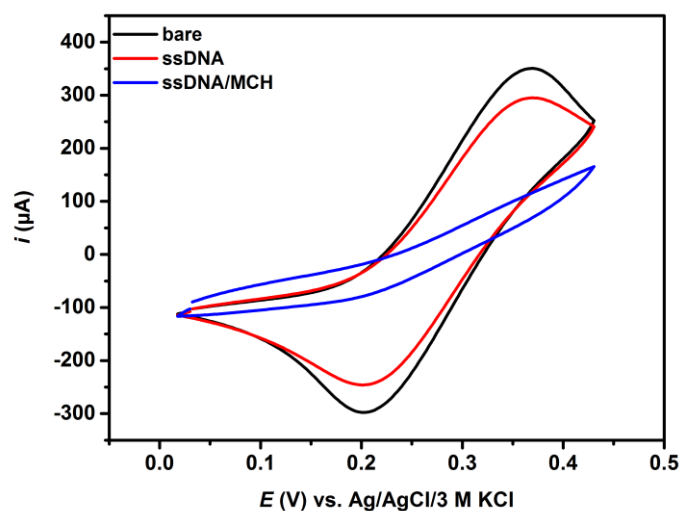


Figure 4.16. CV characterization of an Au electrode surface using the 10 mM PB, 20 mM K_2SO_4 containing 5 mM $K_3[Fe(CN)_6]$ and $K_4[Fe(CN)_6]$ at a scan rate of 100 mV/s.

Figure 4.16 shows a representative CV after each modification step, where the passivation of the electrode surface increases after each immobilization step. To form dsDNA on the SSV surface, the ssDNA/MCH modified surface was incubated in Cy3-labelled target DNA solution for 10 min (Figure 4.17). After the hybridization step, a SERS spectrum was collected from the SSV surface by using the predefined optimized parameters.

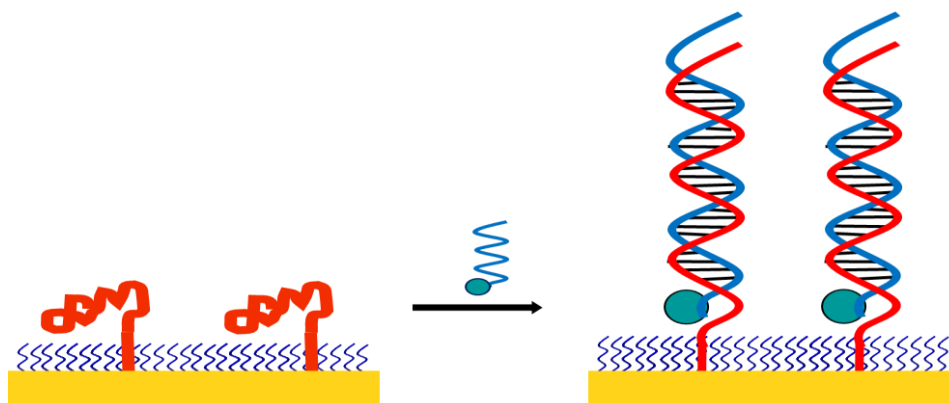


Figure 4.17. Schematic representation of the target labeled DNA hybridization.

In order to optimize the coverage of pDNA, the DNA immobilization time was varied. At low pDNA coverages the hybridization efficiency is maximum, however

the absolute signal is low (Figure 4.18). On the other hand, when the pDNA coverage is too high the hybridization efficiency decreases and with this also the hybridization signal (Figure 4.19). Therefore, it is important to optimize the pDNA in the way that the hybridization efficiency remains maximum but that the absolute amount of immobilized pDNA is also maximum. This was obtained for the immobilization of pDNA using the potential-assisted immobilization method for 2 min (Figure 4.20).

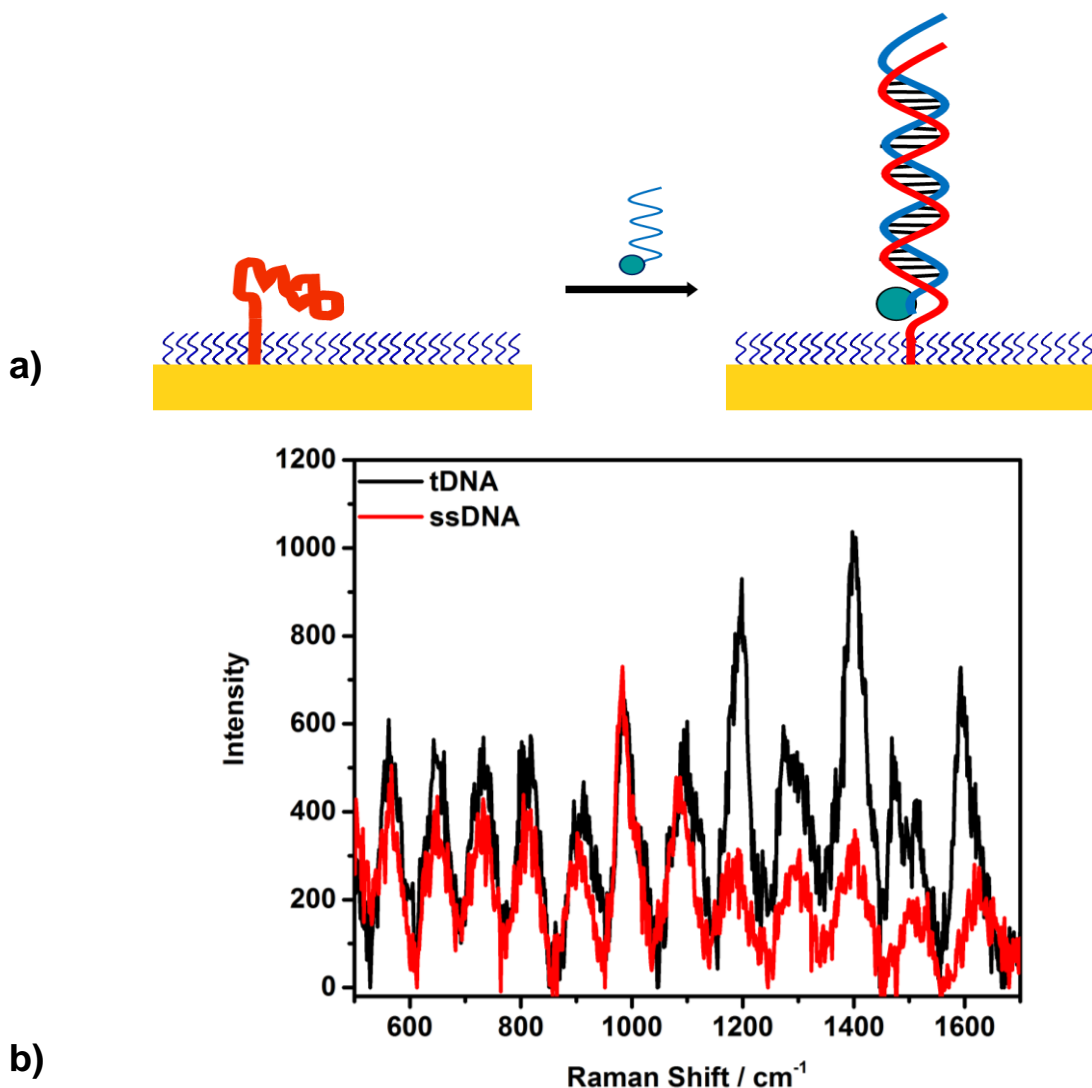


Figure 4.18. ssDNA immobilization using the potential assisted method for 1 min, and Cy3-labeled tDNA by incubating for 10 min. a) schematic representation of DNA hybridization b) SERS spectrum, the laser power at 1.58 mW using a 660 nm excitation laser.

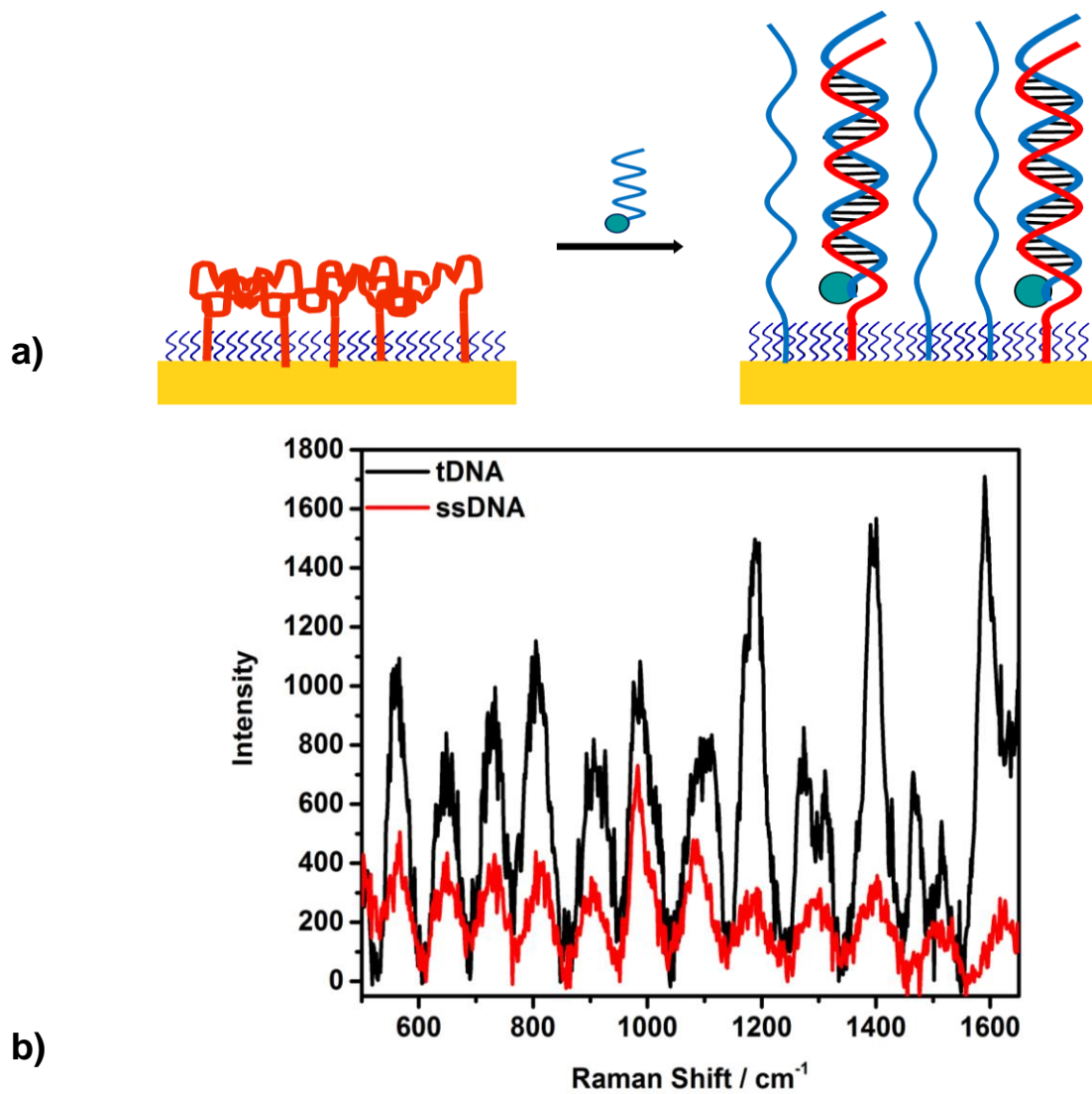


Figure 4.19. Immobilization of ssDNA (3 min) and Cy3-labelled tDNA with incubation (10 min) a) schematic representation b) SERS spectrum was recorded at a laser power at 1.58 mW using a 660 nm excitation laser and an accumulation time of 10 s.

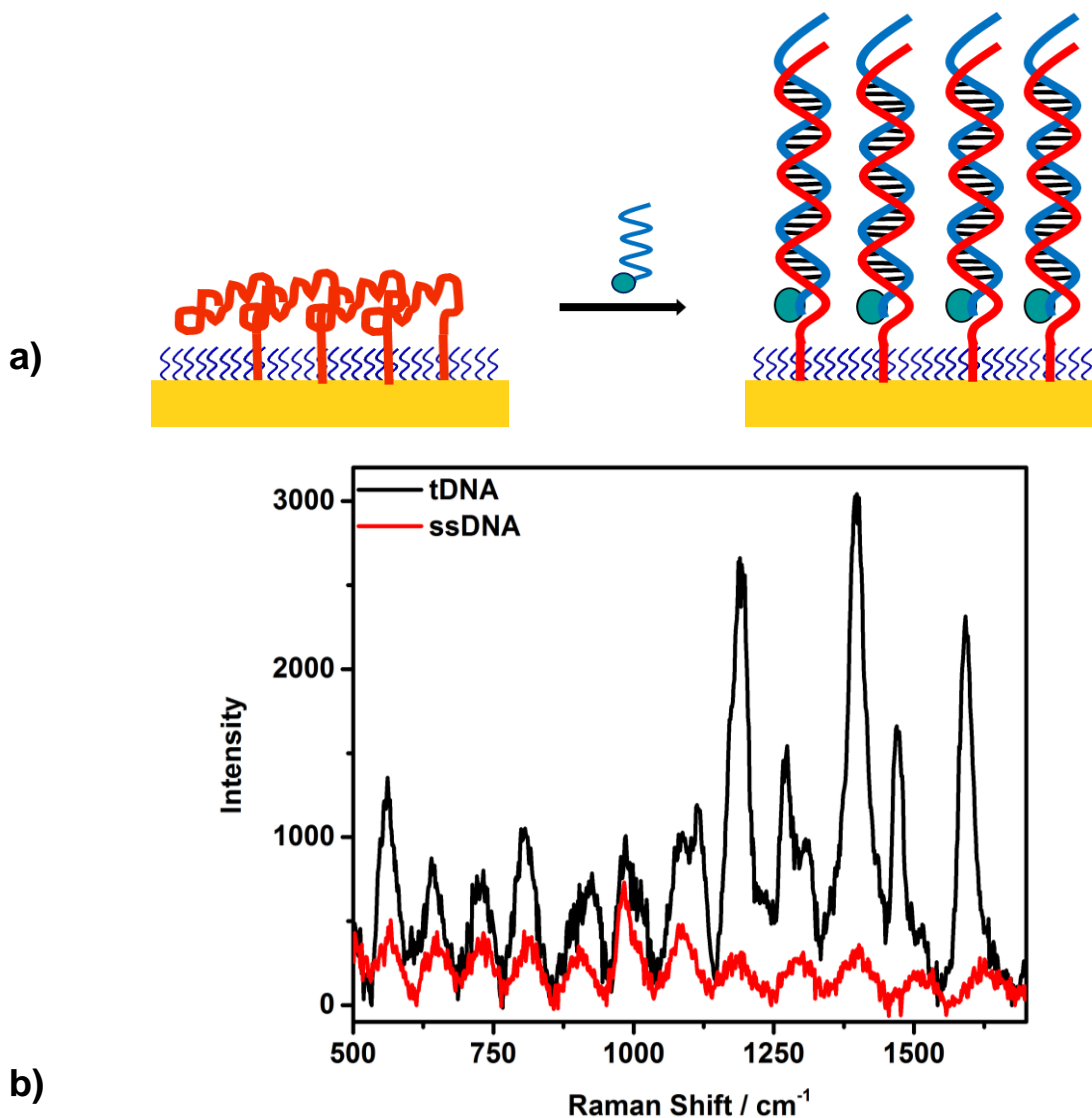


Figure 4.20. ssDNA immobilization (2 min) and tDNA with Cy3-labelled incubation (10 min) a) scheme presenting the DNA sensor b) the detection of the DNA duplex at the surface of a sphere segment void substrate. The spectra was recorded with 10 s acquisition and a 660 nm excitation laser.

Due to the absence of a dye in ssDNA, Raman peaks were observed only after formation of dsDNA with Cy3-labelled tDNA on the SSV surface. Characteristic peaks for Cy3 were observed at 1397 and 1591 cm^{-1} [54].

4.3.2. Electrochemically Driven DNA Dehybridization

The aim of this part of the thesis was to investigate dsDNA melting on SSV surfaces and define the melting potential for the oligonucleotides [44]. After

hybridization, a SERS spectrum was initially recorded at OCP and afterwards a negative constant potential was applied to the SSV surfaces for 20 s, followed by a second SERS measurement. A stepwise increase of the negative potential was performed with a SERS measurement between each step as it is schematically depicted in Figure 4.21. The potential was increased gradually until no signal was observed from the Cy3-tDNA.

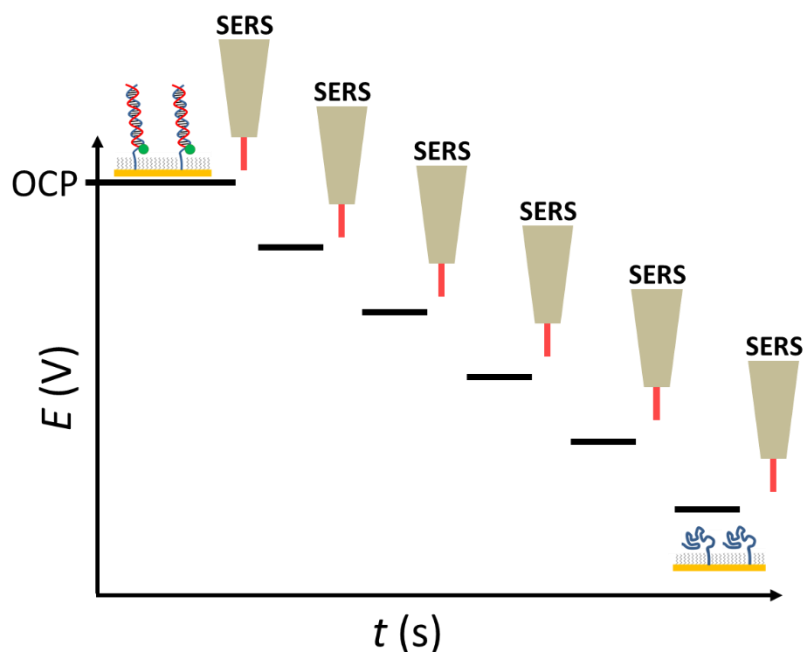


Figure 4.21. Schematic representation of the potential melting curve experiment sequence.

To investigate whether the observed signal loss originates solely from the hybridization or both hybridization combined with desorption of Au-S bond (complete removal of DNA from the surface), the same procedure was performed using labelled pDNA. Initially, the SERS signal was measured at OCP for the Cy3-pDNA modified surface and the stepwise increase of the negative potential was performed with SERS measurements in between until no signal was observed. In Figure 4.22 the ssDNA desorption curve and the dsDNA melting analysis are presented together. It can be seen that the dehybridization starts around a potential of -1.1 V vs. Ag/AgCl (3 M KCl). An important point is that the pDNA desorption does not start at this potential, implying that the signal loss is only due to the dehybridization and that the pDNA film on the surface is stable at this

potential. Furthermore, a potential of -1250 mV vs. Ag/AgCl (3 M KCl) was selected as the DNA dehybridization potential at which an efficient dsDNA dehybridization occurs and no pDNA desorption is observed. At potentials higher than this a signal loss in the dsDNA melting curve obviously originates from both dehybridization and desorption of ssDNA from the electrode surface.

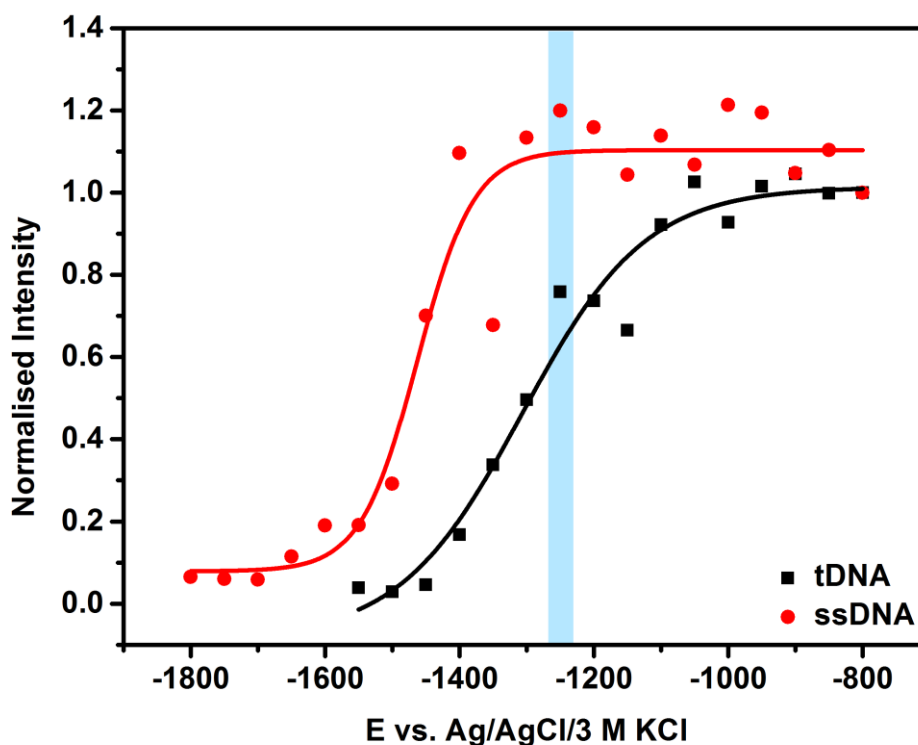


Figure 4.22. dsDNA melting curve and ssDNA desorption curve as a function of the applied potential. Experiment was performed in 10 mM PB buffer containing 450 mM K_2SO_4 .

A defined dehybridization potential was then used to follow the potential-assisted dehybridization of fully matched and single mismatched dsDNA (Figure 4.23). By employing the developed in-situ Raman cell, SERS spectra were collected after each potential application of 1 min.

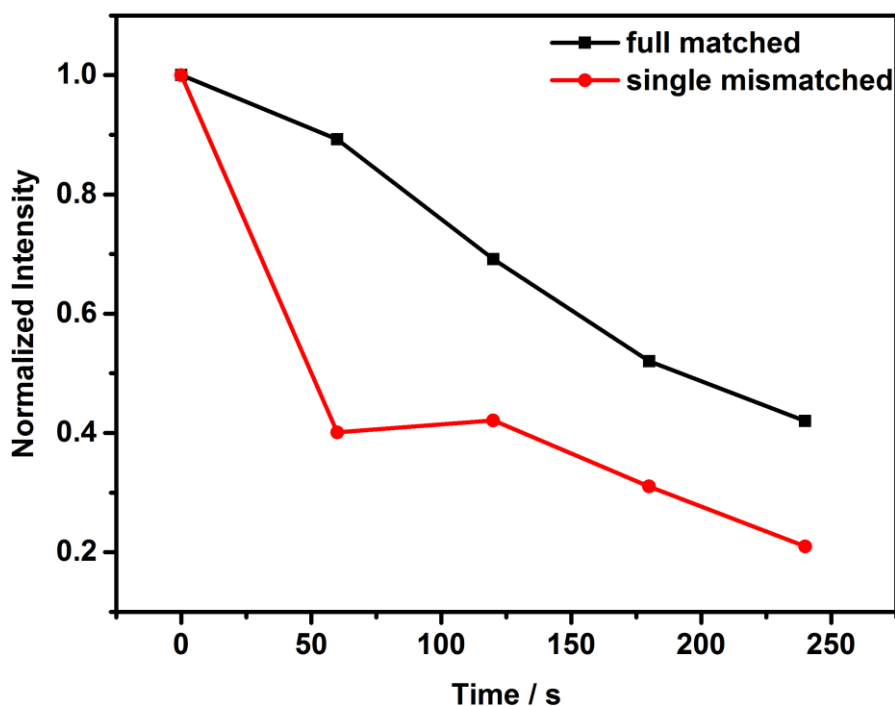


Figure 4.23. DNA dehybridization kinetics of a fully matched and a single mismatched dsDNA. The applied potential was set at -1250 mV vs. Ag/AgCl (3 M KCl) in 10 mM PB buffer containing 450 mM K₂SO₄.

After 60 s of potential assisted DNA dehybridization, 10 % of full matched dsDNA was dehybridized. On the other hand, approximately 60 % of single mismatched dsDNA was dehybridized. 57% of fully matched dsDNA dehybridized after 240 s, while a dehybridization of 80 % of single mismatched dsDNA occurred after this period. Thus, we showed that SNP detection may be achieved in only 60 s by comparing dsDNA dehybridization kinetics with the fully matched dsDNA.

4.3.4. Reproducibility

In order to investigate the reproducibility and reusability of the designed sensor, dsDNA was dehybridized and rehybridized 3 times using the same electrode. As defined earlier a potential of -1250 mV vs. Ag/AgCl (3 M KCl) was used as the DNA dehybridization potential which was applied for 240 s. After each dehybridization and rehybridization step, a SERS spectrum was collected.

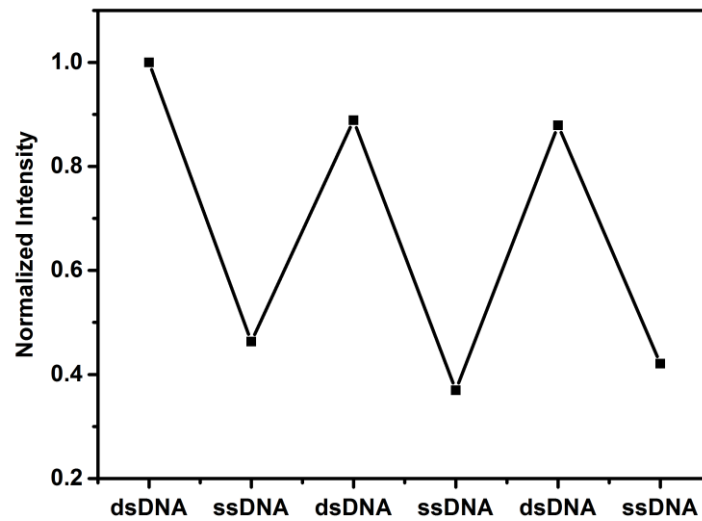


Figure 4.24. Reproducibility of the developed DNA sensor. The spectrum used is from the Cy3 labelled tDNA and the non-labelled probe DNA.

After the first rehybridization the Raman intensity recovered was 90 % of the initial value. However, no further decrease of the signal was observed. This can be attributed to some rearrangement of the surface. It is important that after this the signal does not decrease anymore. Dehybridization steps caused the signal decrease of 55-60 %, comparable with the result from the Figure 4.24. Thus, the reproducibility of the designed DNA sensor is acceptable.

5. CONCLUSIONS

Wide range of human diseases originates from single nucleotide polymorphism. Therefore, SNP detection is of significant importance for the future of medicine. Due to its sensitivity, SERS technique has a great potential for the application in DNA biosensors.

One of the aims of the thesis was to find an efficient and reproducible procedure for fabrication of nanovoids SERS substrates that cause high enhancement of SERS signals. Langmuir-Blodgett method was employed to prepare homogeneous and reproducible templates using different sizes of polymer beads. Fast and efficient optimization of the Au thickness was achieved by means of bipolar electrochemistry, creating a gold deposit gradient. After the Au thickness gradient formation, the templates were dissolved from the electrode surfaces, and the SSV assembled electrodes were modified with a Raman reporter molecule (4-NTP). The ideal SSV structure was found by scanning with a Raman probe. The SERS scanning measurements showed that the SSV structures which were prepared with closely-packed 200 nm diameter nanobeads provided the highest SERS intensity. Using SEM showed that the optimal void opening is 183.2 nm and the optimal gold thickness was calculated to be 177.8 nm. Moreover, the optimal Au deposition potential at that spot was measured to be -0.610 V vs. Ag/AgCl/3 M KCl. After investigation of the Au deposition using chronoamperometry it was observed that the duration of the deposition is not the most important parameter in achieving the required reproducibility of the produced nanostructures, but rather the shape of the current-time curve. Namely, the time needed to achieve the desired nanovoids structures differs between samples. This can originate from difference in cleanliness of substrates and/or deposition solution. Therefore, keeping the deposition time constant results in irreproducibility of fabricated structures and with this the SERS intensity. On the other hand, preparing the structures by stopping the deposition after a desired curve shape was obtained resulted in reproducible nanostructures.

The second part of the thesis was focused on the development of a procedure for the differentiation of fully complementary DNA from single mismatched sequences. The designed SERS-based sensor was fabricated using the potential pulse

assisted immobilization method and the hybridization was performed using Cy3-labelled tDNA. Mismatch analysis strategy employed the potential-assisted dehybridization of dsDNA. After optimizing the melting potential the dehybridization kinetics of fully complementary and single mismatched sequences was monitored. DNA dehybridization kinetics was monitored by means of in-situ SERS measurements. Overall, a DNA mismatch analysis method was established with a high reproducibility and it has a big potential for the application in the field of DNA sensors.

REFERENCES

- [1] Zhai, J., Cui, H., Yang, R., DNA based biosensors. *Biotechnology Advances*, 15(1), 43–58, **1997**.
- [2] Sassolas, A., Leca-Bouvier, B.D., Blum, L.J., DNA biosensors and microarrays. *Chemical reviews*, 108(1), 109–139, **2008**.
- [3] Papadopoulou, E., Meneghello, M., Marafini, P., Johnson, R.P., Brown, T., Bartlett, P.N., The effect of temperature on electrochemically driven denaturation monitored by SERS. *Bioelectrochemistry (Amsterdam, Netherlands)*, 106(Pt B), 353–358, **2015**.
- [4] Kelly, K.L., Coronado, E., Zhao, L.L., Schatz, G.C., The Optical Properties of Metal Nanoparticles. *The Journal of Physical Chemistry B*, 107(3), 668–677, **2003**.
- [5] Aizpurua, J., Hanarp, P., Sutherland, D.S., Kall, M., Bryant, G.W., Garcia de Abajo, F J, Optical properties of gold nanorings. *Physical review letters*, 90(5), 57401, **2003**.
- [6] Cintra, S., Abdelsalam, M.E., Bartlett, P.N., Baumberg, J.J., Kelf, T.A., Sugawara, Y., Russell, A.E., Sculpted substrates for SERS. *Faraday Discuss*, 132), 191–199, **2006**.
- [7] Roberts, G.G., Langmuir-Blodgett films, Plenum Press, **1990**.
- [8] Ulman, A., An introduction to ultrathin organic films: From Langmuir-Blodgett to self-assembly, Academic Press, **1991**.
- [9] Hussain, S.A., Bhattachar, D., Langmuir-Blodgett Films and Molecular Electronics. *Modern Physics Letters B*, 23(29), 3437–3451, **2009**.
- [10] Tredgold, R.H., The physics of Langmuir-Blodgett films. *Reports on Progress in Physics*, 50(12), 1609–1656, **1987**.
- [11] Biolin Scientific <http://www.biolinscientific.com/technology/l-lb-ls-technique/> (Aralık, **2016**).
- [12] Schlücker, S., Surface enhanced Raman spectroscopy: Analytical, biophysical and life science applications, Wiley-VCH, **2011**.

- [13] Ferraro, J.R., Nakamoto, K., Brown, C.W., *Introductory Raman spectroscopy*, Academic Press, **2003**.
- [14] Lewis, I.R., Edwards, H.G.M., *Handbook of raman spectroscopy*, Marcel Dekker, **2001**.
- [15] Gauglitz, G., Vo-Dinh, T., Moore, D.S., *Handbook of spectroscopy*, Wiley-VCH, **2003**.
- [16] Smith, E., Dent, G., *Modern Raman Spectroscopy - A Practical Approach*, John Wiley & Sons, Ltd, **2004**.
- [17] McNay, G., Eustace, D., Smith, W.E., Faulds, K., Graham, D., Surface-enhanced Raman scattering (SERS) and surface-enhanced resonance Raman scattering (SERRS): a review of applications. *Applied spectroscopy*, 65(8), 825–837, **2011**.
- [18] Fleischmann, M., Hendra, P.J., McQuillan, A.J., Raman spectra of pyridine adsorbed at a silver electrode. *Chemical Physics Letters*, 26(2), 163–166, **1974**.
- [19] Campion, A., Kambhampati, P., Surface-enhanced Raman scattering. *Chemical Society Reviews*, 27(4), 241, **1998**.
- [20] Kneipp, K., Kneipp, H., Itzkan, I., Dasari, R.R., Feld, M.S., Surface-enhanced Raman scattering and biophysics. *Journal of Physics: Condensed Matter*, 14(18), R597-R624, **2002**.
- [21] Moskovits, M., Surface-enhanced spectroscopy. *Reviews of Modern Physics*, 57(3), 783–826, **1985**.
- [22] Brown, R.J.C., Milton, M.J.T., Nanostructures and nanostructured substrates for surface-enhanced Raman scattering (SERS). *Journal of Raman Spectroscopy*, 39(10), 1313–1326, **2008**.
- [23] Sharma, B., Frontiera, R.R., Henry, A.-I., Ringe, E., van Duyne, R.P., SERS. *Materials Today*, 15(1-2), 16–25, **2012**.
- [24] Freeman, R.G., Grabar, K.C., Allison, K.J., Bright, R.M., Davis, J.A., Guthrie, A.P., Hommer, M.B., Jackson, M.A., Smith, P.C., Walter, D.G.,

- Natan, M.J., Self-Assembled Metal Colloid Monolayers: An Approach to SERS Substrates. *Science (New York, N. Y.)*, 267(5204), 1629–1632, **1995**.
- [25] Baltog, I., Primeau, N., Reinisch, R., Coutaz, J.L., Surface enhanced Raman scattering on silver grating. *Applied Physics Letters*, 66(10), 1187, **1995**.
- [26] Abdelsalam, M.E., Bartlett, P.N., Baumberg, J.J., Cintra, S., Kelf, T.A., Russell, A.E., Electrochemical SERS at a structured gold surface. *Electrochemistry Communications*, 7(7), 740–744, **2005**.
- [27] Nie, S., Probing Single Molecules and Single Nanoparticles by Surface-Enhanced Raman Scattering. *Science*, 275(5303), 1102–1106, **1997**.
- [28] Tao, A.R., Huang, J., Yang, P., Langmuir-Blodgett of nanocrystals and nanowires. *Accounts of Chemical Research*, 41(12), 1662–1673, **2008**.
- [29] Bartlett, P.N., Birkin, P.R., Ghanem, M.A., Electrochemical deposition of macroporous platinum, palladium and cobalt films using polystyrene latex sphere templates. *Chemical Communications*, 17), 1671–1672, **2000**.
- [30] Netti, M.C., Coyle, S., Baumberg, J.J., Ghanem, M.A., Birkin, P.R., Bartlett, P.N., Whittaker, D.M., Confined Surface Plasmons in Gold Photonic Nanocavities. *Advanced Materials*, 13(18), 1368–1370, **2001**.
- [31] Kayran, Y.U., Eßmann, V., Grütze, S., Schuhmann, W., Selection of Highly SERS-Active Nanostructures from a Size Gradient of Au Nanovoids on a Single Bipolar Electrode. *ChemElectroChem*, 3(3), 399–403, **2016**.
- [32] Fosdick, S.E., Knust, K.N., Scida, K., Crooks, R.M., Bipolar electrochemistry. *Angewandte Chemie (International ed. in English)*, 52(40), 10438–10456, **2013**.
- [33] Mavre, F., Anand, R.K., Laws, D.R., Chow, K.-F., Chang, B.-Y., Crooks, J.A., Crooks, R.M., Bipolar electrodes: a useful tool for concentration, separation, and detection of analytes in microelectrochemical systems. *Analytical chemistry*, 82(21), 8766–8774, **2010**.
- [34] Braun, T.M., Schwartz, D.T., Localized Electrodeposition and Patterning Using Bipolar Electrochemistry. *Journal of the Electrochemical Society*, 162(4), D180-D185, **2015**.

- [35] Eßmann, V., Jambrec, D., Kuhn, A., Schuhmann, W., Linking glucose oxidation to luminol-based electrochemiluminescence using bipolar electrochemistry. *Electrochemistry Communications*, 50), 77–80, **2015**.
- [36] Wang, J., From DNA biosensors to gene chips. *Nucleic acids research*, 28(16), 3011–3016, **2000**.
- [37] Alberts, B., *Molecular biology of the cell*, Garland Science, **2002**.
- [38] Nimse, S.B., Song, K., Sonawane, M.D., Sayyed, D.R., Kim, T., Immobilization techniques for microarray: challenges and applications. *Sensors (Basel, Switzerland)*, 14(12), 22208–22229, **2014**.
- [39] Drummond, T.G., Hill, M.G., Barton, J.K., Electrochemical DNA sensors. *Nature biotechnology*, 21(10), 1192–1199, **2003**.
- [40] PALEČEK, E., Oscillographic Polarography of Highly Polymerized Deoxyribonucleic Acid. *Nature*, 188(4751), 656–657, **1960**.
- [41] Papadopoulou, E., Gale, N., Thompson, J.F., Fleming, T.A., Brown, T., Bartlett, P.N., Specifically horizontally tethered DNA probes on Au surfaces allow labelled and label-free DNA detection using SERS and electrochemically driven melting. *Chemical Science*, 7(1), 386–393, **2016**.
- [42] Valenta, P., Nornberg, H.W., The electrochemical behaviour of DNA at electrically charged interfaces. *Biophysics of Structure and Mechanism*, 1(1), 17–26, **1974**.
- [43] Paleček, E., Normal pulse polarography of double-helical DNA. *Collection of Czechoslovak Chemical Communications*, 39(12), 3449–3455, **1974**.
- [44] Johnson, R.P., Gale, N., Richardson, J.A., Brown, T., Bartlett, P.N., Denaturation of dsDNA immobilised at a negatively charged gold electrode is not caused by electrostatic repulsion. *Chemical Science*, 4(4), 1625, **2013**.
- [45] Piunno, P.A.E., Krull, U.J., Hudson, R.H.E., Damha, M.J., Cohen, H., Fiber-Optic DNA Sensor for Fluorometric Nucleic Acid Determination. *Analytical Chemistry*, 67(15), 2635–2643, **1995**.

- [46] Peng, H.-I., Miller, B.L., Recent advancements in optical DNA biosensors: exploiting the plasmonic effects of metal nanoparticles. *The Analyst*, 136(3), 436–447, **2011**.
- [47] Laing, S., Gracie, K., Faulds, K., Multiplex in vitro detection using SERS. *Chemical Society reviews*, 45(7), 1901–1918, **2016**.
- [48] Harpster, M.H., Zhang, H., Sankara-Warrier, A.K., Ray, B.H., Ward, T.R., Kollmar, J.P., Carron, K.T., Mecham, J.O., Corcoran, R.C., Wilson, W.C., Johnson, P.A., SERS detection of indirect viral DNA capture using colloidal gold and methylene blue as a Raman label. *Biosensors & bioelectronics*, 25(4), 674–681, **2009**.
- [49] Pasta, M., Battistel, A., La Mantia, F., Lead–lead fluoride reference electrode. *Electrochemistry Communications*, 20), 145–148, **2012**.
- [50] Hoogvliet, J.C., Dijkstra, M., Kamp, B., van Bennekom, W.P., Electrochemical Pretreatment of Polycrystalline Gold Electrodes To Produce a Reproducible Surface Roughness for Self-Assembly. *Analytical Chemistry*, 72(9), 2016–2021, **2000**.
- [51] Jambrec, D., Gebala, M., La Mantia, F., Schuhmann, W., Potential-Assisted DNA Immobilization as a Prerequisite for Fast and Controlled Formation of DNA Monolayers. *Angewandte Chemie (International ed. in English)*, 54(50), 15064–15068, **2015**.
- [52] Jambrec, D., Conzuelo, F., Estrada-Vargas, A., Schuhmann, W., Potential-Pulse-Assisted Formation of Thiol Monolayers within Minutes for Fast and Controlled Electrode Surface Modification. *ChemElectroChem*, 3(9), 1484–1489, **2016**.
- [53] Clarke, R.H., Ha, S., Resonance Raman spectroscopy of proflavin (II). *Spectrochimica Acta Part A: Molecular Spectroscopy*, 43(11), 1385–1392, **1987**.
- [54] Long, D.A., Infrared and Raman characteristic group frequencies. Tables and charts George Socrates John Wiley and Sons, Ltd, Chichester, Third Edition, 2001. Price £135. *Journal of Raman Spectroscopy*, 35(10), 905, **2004**.
- [55] Johnson, R.P., Richardson, J.A., Brown, T., Bartlett, P.N., Real-time surface-enhanced Raman spectroscopy monitoring of surface pH during electrochemical melting of double-stranded DNA. *Langmuir : the ACS journal of surfaces and colloids*, 28(12), 5464–5470, **2012**.

CURRICULUM VITAE

Credentials

Name, Surname : Nergis ÇINAR
Place of Birth : Ankara
Marital Status : Single
E-mail : nergiscinar@gmail.com
Address : Hacettepe University, Department of Chemistry,
06800 Beytepe, Ankara, TURKEY

Education

High School : Ankara Ayranci Lisesi
B. Sc. : Anadolu University
M. Sc. : Hacettepe University

Foreign Languages

English : Fluent
German : Beginner

Work Experiences

Area of Experiences

Biosensor, SERS, bipolar electrochemistry, voltammetric techniques Langmuir-Blodgett.

Projects and Budgets

Publications

Oral and Poster Presentations



HACETTEPE UNIVERSITY
GRADUATE SCHOOL OF SCIENCE AND ENGINEERING
THESIS/DISSERTATION ORIGINALITY REPORT

HACETTEPE UNIVERSITY
GRADUATE SCHOOL OF SCIENCE AND ENGINEERING
TO THE DEPARTMENT OF CHEMISTRY

Date: 20/01/2017

Thesis Title / Topic: Detection of DNA Hybridization and Dehybridization with Surface Enhanced Raman Spectroscopy (SERS) by Using Gold Nanovoids Electrodes

According to the originality report obtained by myself/my thesis advisor by using the *Turnitin* plagiarism detection software and by applying the filtering options stated below on 17/01/2017 for the total of 72 pages including the a) Title Page, b) Introduction, c) Main Chapters, d) Conclusion and e) Bibliography sections of my thesis entitled as above, the similarity index of my thesis is 9 %.

Filtering options applied:

1. Bibliography/Works Cited excluded
2. Quotes excluded
3. Match size up to 5 words excluded

I declare that I have carefully read Hacettepe University Graduate School of Science and Engineering Guidelines for Obtaining and Using Thesis Originality Reports; that according to the maximum similarity index values specified in the Guidelines, my thesis does not include any form of plagiarism; that in any future detection of possible infringement of the regulations I accept all legal responsibility; and that all the information I have provided is correct to the best of my knowledge.

I respectfully submit this for approval.

Date and Signature

Name Surname: NERGİS ÇINAR

Student No: N13223192

Department: Chemistry

Program: Masters

Status: Masters Ph.D. Integrated Ph.D.

23/01/2017
Nergis Çinar

ADVISOR APPROVAL

APPROVED

Prof. Dr. Handan YAVUZ ALAGÖZ

(Title, Name Surname, Signature)